Organotypic 3D Decellularized Matrix Tumor Spheroids for High-throughput Drug Screening

Luís P. Ferreira, Vítor M. Gaspar*, Luís Mendes, Iola F. Duarte, João F. Mano*

Department of Chemistry, CICECO – Aveiro Institute of Materials, University of Aveiro, Campus Universitário de Santiago, 3810-193, Aveiro, Portugal

*Corresponding authors:
Dr. Vítor Gaspar
Department of Chemistry, CICECO – Aveiro Institute of Materials
University of Aveiro, Campus Universitário de Santiago
3810-193, Aveiro, Portugal
E-mail: vm.gaspar@ua.pt
Telephone: +351 234370733

Professor João Mano
Department of Chemistry, CICECO – Aveiro Institute of Materials
University of Aveiro, Campus Universitário de Santiago
3810-193, Aveiro, Portugal
E-mail: jmano@ua.pt
Telephone: +351 234370733

Abstract

Decellularized extracellular matrix (dECM) is emerging as a valuable tool for generating 3D *in vitro* tumor models that better recapitulate tumor-stroma interactions. However, the development of dECM-3D heterotypic micro- tumors exhibiting a controlled morphology is yet to be materialized. Precisely controlling microtumors morphologic features is key to avoid an inaccurate evaluation of therapeutics performance during preclinical screening. To address this, herein we employed ultra-low adhesion surfaces for bioengineering organotypic 3D metastatic breast cancer-fibroblast models enriched with dECM microfibrillar fragments, as a bottom-up strategy to include major matrix components and their associated biomolecular cues during the early stages of 3D microtissue spheroids assembly, simulating pre-existing ECM presence in the *in vivo* setting. This biomimetic approach enabled the self-assembly of dECM-3D tumor-stroma spheroids with tunable size and reproducible morphology. Along time, dECM enriched and stroma-rich microtumors exhibited necrotic core formation, secretion of key biomarkers and higher cancer-cell specific resistance to different chemotherapeutics in com- parison to standard spheroids. Exometabolomics profiling of dECM-Spheroid *in vitro* models further identified important breast cancer metabolic features including glucose/pyruvate consumption and lactate excretion, which suggest an intense glycolytic activity, recapitulating major hallmarks of the native microenvironment. Such organotypic dECM-enriched microtumors overcome the morphologic variability generally associated with cell-laden dECM models, while providing a scalable testing platform that can be foreseeable leveraged for high- throughput screening of candidate therapeutics.

1. Introduction

Leveraging 3D *in vitro* solid tumor models for anti-cancer therapeutics preclinical screening has received increasing attention owing to their recognized potential to overcome the limitations of 2D monolayer cell cultures, as well as the cost and ethical issues associated with human xenograft animal models [1–3]. Biomimetic multicellular 3D tumor spheroids are among the most valuable disease models owing to their ability to recapitulate the three-dimensional cellular distribution, tumor-stroma multicellular components, oxygen/nutrient/pH gradients and the biochemical cues existing in *in vivo* solid tumor microenvironment (TME). Spheroids ease of assembly, cost-effectiveness, reproducible morphology and possibility to be included in high-content bioimaging systems, or high-throughput static/dynamic microfluidic platforms render them as highly valuable tools for accelerating pre- clinical therapeutics discovery and screening [4–6]. However, despite their potential for recapitulating cell-cell interactions, they are still intrinsically limited since no pre-existing extracellular matrix (ECM) is included during cell aggregation in non-adherent conditions, thus not recapitulating a key hallmark of the native TME [1,7,8].

During the early stages of tumor development and disease progression pre-existing tissue ECM is recognized to exert a major influence in tumorigenesis, contributing overtime to resistance and metastasis [9–13]. While scaffold-free spheroid models are able to deposit their own ECM in culture, the *de novo* formed matrix is generated in a cell line and culture dependent manner, demanding significant periods to accumulate in physiologically relevant amounts [14,15]. Moreover, significant variations in deposited ECM are observed just by varying spheroid assembly methodology [14,16]. Therefore, although 3D cultured cells-derived extracellular matrices are reported to be more representative than the ECM obtained in monolayer cultures, these models still fail to recapitulate the full biomolecular composition of tissue-specific CM [17–19]. This lack of tissue/tumor-specific ECM representation can lead to uncharacteristic organization and phenotypes, as well as altered signaling profiles in cancer and associated stromal cells when compared to more complex models containing matrix-mimetic scaffolds [1,7,8].

Recent studies have shown that inclusion of spheroids within ECM mimetic matrix leads to increase recapitulation of tumor specific hall- marks [20]. Importantly, has been previously demonstrated ECM com- ponents inclusion during spheroid aggregation can exert distinct effects when compared to spheroids cultured in ECM mimetic scaffolds [21,22]. The inclusion of ECM components during spheroids assembly improves their potential as *in vitro* microtumor surrogates by recapitulating cancer/stromal cells native crosstalk with the supporting ECM. Such dynamic cell-matrix interactions are recognized to generate a pro-tumoral microenvironment, which promotes the onset of metastasis

and multi-drug resistance [23–26]. The development of 3D models including TME mimetic populations and the dynamic extracellular supporting matrix is therefore envisioned to provide significant advances in *in vitro* tumor modeling. To address this, lessons can be used from high-throughput evaluation of the performance of biomaterials and cells in tissue engineering strategies [27]. ECM-mimetic biomaterial scaffolds either in the form of microparticles or cell-laden hydrogels have been widely explored [7]. In general, microparticle and hydrogel models only recapitulate single components of tumor ECM (e.g., collagen, fibronectin, hyaluronan) and are unable to fully recreate ECM microfibrillar fragments architecture and topographic features.

Decellularized extracellular matrix (dECM) is being increasingly employed as a biomaterial for *in vitro* disease modeling as it provides a tissue-specific bioactive platform, which preserves key biophysical/ biochemical cues that support cell adhesion/proliferation and activate critical cell-matrix signaling pathways [28]. Up to now, few dECM-based breast cancer models have been developed, with most studies employing enzymatically digested dECM and post processing into soft-sponges, or to self-gelling and/or hybrid 3D hydrogels combined with other biomaterials [29,30]. Despite most reports describing valuable models to perform in-depth studies of cancer cell-ECM interactions, most of them fall-short on fabricating easily scalable and morphologically reproducible microtumors on which pre-clinical drug screening can be performed. As recently discussed elsewhere, most of breast cancer dECM-based models are assembled via random reseeding decellularized scaffolds with different cells [31]. Moreover, several models employ non-mammary tissues derived dECM (e.g., lung, liver, etc) [29,32–39]. Other approaches also comprise pepsin digested dECM-based hydrogels [37,40], hybrid scaffolds combining digested dECM with synthetic or nature-derived biomaterials [41], or the manufacture of dECM-based bioinks, (of porcine and human origin), developed for bioprinting breast cancer models [41,42]. Although these strategies provide advantages the high-throughput manufacture of such models, the unpredictability of cell-laden dECM hydrogel models, and issues associated with cells sedimentation during printing are yet to be overcome. These factors limit the fabrication of unitary and dense 3D microtumors, because cancer cells generally form highly random ag- glomerates with poorly controllable morphology within hydrogels network [29]. This is a critical parameter, considering that the cellular agglomeration state of cancer cells in hydrogels (e.g., cell-laden or spheroid-laden) may affect drug screening readouts [21]. Controlling the morphological features of *in vitro* generated microtumors is therefore crucial for assuring a correct evaluation of candidate therapeutics bio- performance in preclinical testing stages.

To address such bottlenecks, we employed bottom-up bioengineering approaches [43] for

generating metastatic breast cancer models comprising key tumor components, namely: (i) breast tissue-derived porcine dECM, (ii) cancer cells and (iii) stromal fibroblasts, which constitute a TME-mimetic platform. In particular, we propose a modified liquid-overlay technique, to enable the assembly of dECM-enriched spheroids (dECM-Spheroids) in high-throughput compatible platforms. *In vitro* generated monotypic and heterotypic dECM-Spheroids exhibited a reproducible morphology, necrotic core and differential resistance to chemotherapeutics. The produced triple component dECM-Spheroids recapitulated the invasive profile of metastatic breast cancer cells and evidenced exometabolomic signatures similar to those observed for human tumors. Overall, dECM-3D cancer-stroma microtumors mimic key hallmarks of breast cancer, constituting a valuable platform that can be adapted for both fundamental cancer studies of for screening candidate therapeutics.

2. Materials and Methods

2.1.Materials

Ultra-Low adhesion (ULA) U-bottom 96-well plates (Corning™, 7007), Fetal Bovine Serum = (FBS, E.U. approved, South America origin), RPMI 1640 medium (RPMI 1640), Dulbecco's Modified Eagle Medium-High Glucose (DMEM-HG), Low serum supplement kit (LSGS), phosphate buffered saline, without Ca^{2+} and Mg^{2+}(D-PBS, pH 7.4), Antibiotic-Antimycotic (ATB, Gibco® - 10,000 U/mL of penicillin, 10,000 µg/mL of streptomycin, and 25 µg/mL of Amphotericin B), TrypLE™ Express, Calcein-AM, Propidium Iodide (PI), DiI and DiO were purchased from Thermofisher Scientific (Alfagene, Carcavelos, Portugal). Trypsin-EDTA detaching solution and Hexamethyldisilazane (HMDS) was obtained from Laborspirit (Merck-Sigma, Portugal). Total Collagen Assay Kit (Perchlorate-Free) was obtained from Abcam (Cambridge, UK). Blyscan™ Sulfated Glycosaminoglycan Assay Kit was obtained from Biocolor (Biocolor Life Science Assays, Carrickfergus, UK).

2.2.Methods

2.2.1. Tissue decellularization

Porcine-derived tissues were freshly obtained from a local slaughterhouse and immediately frozen at 80 °C to prevent any deterioration. Tissue decellularization was carried out after overnight thawing at 4 °C. Breast tissue areas immediately adjacent to the mammary gland were then surgically excised and cut into smaller sub-sections (3–5 mm), for posterior processing. Prior to decellularization, porcine mammary-

derived adipose and connective tissues were washed three times in D- PBS, and then decellularized by immersion in Triton-X 100 (1% v/v) containing ammonium hydroxide (NH_4OH, 0.1% w/v) during 48 h, at room temperature (RT). Decellularized tissue was then washed three times in D-PBS to remove excess Triton-X 100 and NH_4OH. Afterwards, dECM was immersed in a peracetic acid solution 1% (v/v) for 10 min, and washed twice with D-PBS containing a 1% (v/v) ATB solution. The sterilized decellularized tissue was recovered by centrifugation and freeze-dried at -86 °C (Telstar LyoQuest), over a period of 14 days.

2.2.2. Decellularized tissue mechanical homogenization

Breast-derived dECM homogenization into 3D microfibrillar fragments was performed by mechanical disruption, as previously described for collagen microfibrillar fragments production [44]. Prior to homogenization, freeze-dried dECM was cooled to 4 °C and resuspended in cold Phosphate Buffered Saline (PBS, 10x solution). The resulting dECM colloidal dispersion was then homogenized by using an Ultra-Turrax (T 18 digital Ultra-Turrax®, equiped with an S 18N-19 G dispersing probe), during 2 min, at 18,000 rpm (Fig. 1A and B). dECM microfibrils were then frozen and freeze-dried at 86 °C (Telstar LyoQuest), over a period of 14 days.

2.2.3. Decellularized microtissues biochemical characterization

As an initial characterization of the decellularization process, the DNA content of dECM fibrils was quantified by using the Quant-iT™ Picogreen™ dsDNA assay. Briefly, isolated dECM was digested in Papain solution (20 mg/mL, in 0.2 M sodium phosphate buffer, pH 6.4), during 24 h, at 65 °C. The resulting homogenate was then centrifuged at 500 g for 10 min, to remove any large sediments. The supernatant was then incubated with Picogreen™ following the manufacturer's instructions and DNA-Picogreen conjugates fluorescence was measured in a microplate reader (Synergy HTX, λ_{ex} 480 nm, λ_{em} 560 nm). An additional qualitative screening was performed through DAPI nuclear staining (10 μM) of non-minced decellularized tissue blocks by incubating the samples for 10 min, at RT, followed by three washes with D- PBS. Tissue samples were the imaged in a widefield fluorescence microscope (Zeiss Imager M2, Carl Zeiss, Germany).

The collagen and proteoglycan content of native ECM and dECM were determined by using the Abcam™ Total Collagen Assay Kit (Perchlorate-Free), and Blyscan™ Sulfated Glycosaminoglycan Assay, respectively. For collagen analysis ECM and dECM samples were subjected to acid hydrolysis (HCL, 10 M), at 120 °C, for 1 h to yield free hydroxyproline residues. The pH was then adjusted using NaOH (10 M) and the digested samples were crystalized at 65 °C. Following the manufacturer's instructions, collagen content was obtained through hydroxyproline

residue oxidization. The resulting chromophore product absorbance was measured at λ = 560 nm. Regarding glycosaminoglycans analysis, ECM and dECM the samples were digested in Papain solution (20 mg/mL) at 65 °C for 18 h, under stirring. s-Glycosaminoglycans were conjugated with the Blyscan™ kit following manufacturer's guidelines and the absorbance was quantified in a plate reader (Synergy HTX, λ = 656 nm). In all assays dECM mass was normalized against that of freeze-dried non-decellularized ECM, as described in the literature [45]. All assays were performed in triplicate, with a total of 3 experimental replicates per analysis.

2.2.4. Scanning electron microscopy analysis

Scanning electron microscopy (SEM) analysis was performed to evaluate dECM post-decellularization and homogenization. Briefly, small dECM sections (<2 mm) were initially washed in distilled water and then fixed in PFA 4% (v/v, in dH_2O), at RT, for 24 h, before being dehydrated in graded concentrations of ethanol (25%, 50%, 75%, 100%), for 30 min, at RT. Following ethanol dehydration, dECM samples were immersed in growing concentrations of HMDS, (50%, 100% Ethanol-HMDS) for 30 min, before being carefully mounted into aluminum stubs using double sided adhesive carbon tape (Agar Scientific, Essex, UK), and allowed to dry overnight. Samples were then sputter coated with gold/palladium and imaged in a benchtop scanning electron microscopy (SEM) or in a Hitachi S-4100 microscope. Analysis of fibers diameter was performed by using a well-established image analysis algorithm (DiameterJ 1.08), ImageJ (v. 1.52, NIH, USA).

2.2.5. Cell culture

All cell lines were manipulated in aseptic conditions and cultured at 37 °C in humidified temperature-controlled incubators with a 5% CO_2 atmosphere. Triple negative breast cancer derived cell line MDA-MB- 231 (ATCC® HTB-26™) was cultured in DMEM-HG medium supplemented with 10% (v/v) FBS and 1% (v/v) ATB. MDA-MB231 reporter cell line expressing Luc and GFP (BioCat SL018-GVO-GC) was cultured during expansion in RPMI-1640 medium supplemented with 10% (v/v) FBS. Prior to spheroid culture MDA-MB-231-Luc-GFP reporter cells were expanded once in fully supplemented DMEM-HG. Luminal A breast cancer lineage MCF-7 was cultured in DMEM-HG medium supplemented with 10% (v/v) FBS and 1% (v/v) ATB, and T47D was cultured in RPMI-1640 medium supplemented with 10% (v/v) FBS and 1% (v/v) ATB. The human primary dermal fibroblasts cell line (HF) (ATCC®-PCS-201- 012™) was cultured in M106 supplemented with Low serum supplement kit (LSGS S-003-10), and 1% (v/v) ATB. Cell expansion was per- formed in monoculture conditions in adherent culture T-flasks. Upon attaining approximately 80–85% confluency, cells were recovered for dECM-Spheroids production by using Trypsin-EDTA.

2.2.6. dECM-3D tumor spheroids assembly

To generate dECM-3D microtumors with well-defined morphological characteristics we propose an innovative modification to the liquid overlay technique that involves sequential seeding/centrifugation of homogenized dECM and multiple cell types in ultra-low adhesion U-shaped substrates. Before cell seeding, freeze-dried dECM microfibrillar fragments were resuspended in complete DMEM-HG cell culture medium, seeded on 96-well Ultra-low adhesion plates (ULA) and centrifuged for 15 min (1200 g, RT). Afterwards cancer or cancer-stromal co- cultured cells were seeded on pelleted dECM microfibrillar fragments and centrifuged for 10 min (500 g, RT). The resulting cell-stromal models were cultured for 14 days. To better recapitulate the tumor microenvironment stromal ECM and the cellular heterogeneity of native breast tumors different parameters, including: (i) initial cell seeding density, (ii) cell-to-cell ratio and (iii) the amount of dECM-to-cell density ratio, were optimized as described in Table 1. This methodology assures the inclusion of key cancer-stromal elements of the tumor microenvironment, while allowing the generation of morphologically defined 3D solid tumor models. Control, monocultured spheroids (MDA-MB-231 cells), and co- cultured 3D microtumors metastatic breast cancer cells and fibroblasts (MDA-MB-231:HF at a 1:2 ratio), were assembled by using the liquid overlay technique as we previously described, with slight modifications [46]. Briefly, to establish cell-only spheroids, cells were detached from culture T-flasks, resuspended to the desired cell seeding density and ratios. and seeded in 96-well ULA plates. Cell-rich microaggregates formation was rapidly assured via mild centrifugation for 10 min (500 g, RT).

Table 1. Summary of parameters used for generating organotypic dECM-3D *in vitro* tumor models.

Culture Type	Cell Lines	Cell-to-cell Ratio	Seeding Density (Cells/well)	dECM (µg/well)	Ref*
Monoculture	MDA-MB-231	**1**	30000	0.0 25 50 100	[47]
Co-culture	MDA-MB-231:HF	**1:2**			[48,49]

*references related to selected cell-to-cell ratios in co-cultured models.

2.2.7. 3D tumor spheroids characterization

3D tumor models size, spheroidal morphology/circularity were analyzed overtime by using an inverted optical contrast microscope (Primovert, Carl Zeiss, Germany) equipped with a transmitted-light Plan-Achromat 4x/0.10/Ph0 objective and a 3MPix color camera. Micro- graphs of control spheroids and dECM-Spheroids were acquired at specific timepoints (1, 7 and 14 days), with a minimum of $n = 6$ spheroids being analyzed per condition and time point. Images were post- processed

and analyzed in open-source software ImageJ (1.52r, Fiji package) by employing a supervised algorithm developed by Ivanov and co-workers [50]. Circularity measurement were performed in accordance with ImageJ supported algorithms, as previously described in the literature [46,51].

2.2.7.1. *3D tumor spheroids cell viability evaluation.* The cell viability of different homotypic (monoculture) and heterotypic (co-culture) 3D tumor spheroids or dECM-Spheroids, was analyzed at specific time- points (7 and 14 days) by using the CellTiter-Glo® cell viability assay (Promega, Madisson, WI, USA), a luminescence-based assay specifically designed to quantify cellular ATP in *in vitro* 3D cellular aggregates, and Live/Dead assay respectively. CellTiter-Glo® assays were performed in accordance with the manufacturer instructions. In brief, spheroids were cultured for 7 or 14 days, before being incubated with a mixture of DMEM-HG and CellTiter-Glo® reagent at a 1:1 ratio. Microtumors samples were then incubated for 5 min under stirring, followed by 25 min of incubation under static conditions, at RT. Luminescence was then measured in 96-well flat-bottom opaque white plates by using a Synergy HTX microplate reader. Non-treated spheroids of each tested condition were used as controls. To analyze the existence of necrotic regions, spheroids of specific time points (7 and 14 days) were incubated with Calcein-AM (CA-AM) (4 μg/mL) and Propidium Iodide (PI) (7 μg/mL) in D-PBS, for 30 min, at 37 °C, 5% CO_2.. Labelled spheroids were then gently washed three times in D-PBS, and immediately analyzed in a widefield fluorescence Axio Imager M2 microscope (Carl Zeiss, Ger- many), equiped with an EC Plan-Neofluar 5x/0.16 objective and an Axiocam 3MPix monochromatic camera.

2.2.7.2. *dECM microfibrillar fragments spatial distribution in spheroids*

To access the spatial distribution of dECM microfibrillar fragments in assembled monotypic and heterotypic 3D breast cancer models dECM was initially labelled with WGA-Alexa Fluor ®594 fluorescent dye that specifically binds to glycosaminoglycan residues, thus allowing to track this component. For this purpose, homogenized dECM was incubated with WGA-Alexa Fluor® 594 overnight, in the dark, and were then centrifuged and washed several times with D-PBS until no fluorescence was detected in the supernatant. Labelled dECM-WGA- Alexa Fluor® 594 - spheroids were then imaged by using a high-resolution Airyscan Laser Confocal Microscope (LSM 880 Airyscan, Carl Zeiss, Germany) equipped with an EC Plan-Neofluar 10x/0.3 objective and a GaAsP-PMT detector. Image processing was performed in Zeiss Zen Blue or Black Software (2019), Imaris or in ImageJ (1.52r) software when applicable.

2.2.8. Cell invasion assays

Aiming to evaluate the ability of breast cancer cells to migrate and invade surrounding tissues, 3D mono and co-culture models with or without dECM microfibers were bioencapsulated in Matrigel™ constructs. Briefly, 3D microtumor spheroids were cultured for a period of 7 days and embedded in Matrigel™ matrix dispersed in µ-Slide Angiogenesis (Ibidi GmbH, Germany). At specific timepoints after encapsulation (days 3 and 7) spheroids were fixed (PFA 4 %, 1 h, RT) and labelled with DAPI, and Flash Phalloidin™ Green 488 (Biolegend, 1:500) for actin labeling. All samples were then visualized in a widefield fluorescence microscope (Axio Imager M2, Carl Zeiss, Germany). In addition, cells migration and invasion were also analyzed through optical contrast microscopy (Primovert, Carl Zeiss, Germany). All micrographs were post-processed with ImageJ (1.52r) software and Zeiss Zen Blue Software (2019).

2.2.9. *Cytotoxic drug screening assays*

To evaluate the effect of dECM inclusion in mono/co-culture models response to anti-cancer drugs, spheroids were cultured for a period of 7 days and incubated with different concentrations of cisplatin, gemcitabine and palbociclib, for 72 h. Cell viability was then evaluated by using 3D CellTiter-Glo® cell viability assay (Promega, Madisson, WI, USA). Cytotoxicity assays analysis with CellTiter-Glo® assays was performed in accordance with the manufacturer instructions and previous descrip- tion. In brief, following compound incubation 3D microtumors were washed with PBS, and then incubated with a mixture of DMEM-HG and CellTiter-Glo® reagent at a 1:1 ratio. Microtumors samples were then incubated for 5 min under stirring, followed by 25 min of incubation under static conditions, at RT. Luminescence was then measured in 96- well flat-bottom opaque white plates by using a Synergy HTX microplate reader. Non-treated spheroids of each tested condition were used as controls.

To evaluate cancer cell specific viability a Firefly reporter assay (BioCat - LF008-GC) was performed in accordance with the manufacturer guidelines, with the exception of cell lysis time and concentration. Considering microtissue size, the lysis solution volume was increased to a volume of 75 µL per spheroid incubated for 15 min under stirring Luc- working solution was then incubated for 20 min, RT, and luminescence was measured in 96-well flat-bottom white plates by using a Synergy HTX microplate reader. Non-treated spheroids of each condition were used as controls.

2.2.10. Exometabolomics profiling of 3D microtumor models

Metabolite consumption and excretion patterns of 3D *in vitro* tumor models were assessed by ^{1}H NMR spectroscopy of medium supernatants. The culture medium was retrieved at day 7 of culture and stored at 80 °C before being processed. To remove interfering proteins, cell culture supernatants were then subjected to a protein-precipitation protocol prior to NMR metabolomics

– analysis, as previously described [52]. In brief, 300 μL of cold methanol 100% (v/v) at —80 °C were added to 100 μL of cell culture supernatant (1:3). The aliquots were incubated at 20 °C for 30 min, and centrifuged at 13,000 g for 20 min, RT. Supernatants were then transferred to another vial, vacuum dried (SpeedVac, Eppendorf) and stored at —80 °C until NMR acquisition. For NMR analysis, the dried samples were resuspended in 600 μL of deuterated phosphate buffer saline (PBS 100 mM, pH 7.4) containing .1 mM 3-(trimethylsilyl) propanoic acid (TSP-d_4), and 550 μL of each sample were then transferred to 5 mm NMR tubes. All samples were analyzed in a Bruker Avance III HD 500 NMR spectrometer (University of Aveiro, Portuguese NMR Network) operating at 500.13 MHz for ^{1}H observation, at 298 K. Standard 1D ^{1}H spectra with water pre-saturation (pulse program 'noesypr1d', Bruker library) were recorded with 32 k points, 7002.801 Hz spectral width, a 2 sec relaxation delay and 512 scans. Spectral processing in TopSpin 4.0.3 (Bruker BioSpin, Rheinstetten, Germany) consisted in cosine multiplication (ssb 2), zero-filling to 64 k data points, manual phasing and baseline correction, and calibration to the TSP-d_4 signal (δ 0 ppm). To aid in metabolite identification, two-dimensional NMR spectra, namely ^{1}H–^{1}H TOCSY, *J*-resolved and ^{1}H–^{13}C HSQC, were also recorded for selected samples. Metabolite assignment was based on matching 1D and 2D spectral information to reference spectra available in Chenomx (Edmonton, Canada), BBIOR- EFCODE-2–0–0 (Bruker Biospin, Rheinstetten, Germany) and HMDB databases [53].

2.2.11. Multivariate analysis

Data matrices containing NMR signal intensities were uploaded into SIMCA-P 11.5 (Umetrics, Umeå, Sweden), where Principal Component Analysis (PCA) and Partial Least Squares-Discriminant Analysis (PLS- DA) were applied. The results were visualized through factorial co-ordinates ('scores') and factorial contributions ('loadings'), colored ac- cording to variable importance to the projection (VIP). For PLS-DA models, Q^2 values, reflecting predictive capability, obtained from sevenfold internal cross validation, were used to assess the robustness of group discrimination. Loadings profiles were generated using the R software version 3.4.1.

For quantitative measurement of metabolic variations, spectral integration of selected signals was carried out in Amix-Viewer 3.9.15 (Bruker Biospin, Rheinstetten, Germany) and the results were expressed as fold change relatively to acellular medium.

2.2.12. ELISA assays

Culture media (CM), obtained from different culture conditions, was centrifuged to remove any

cellular debris and stored at —80 °C prior to analysis. The expression levels of TGF-β1 (Abcam, ab108912 – TGF-β1 Human ELISA Kit), CXCL16 (Invitrogen, Human CXCL16 ELISA Kit, CN:EHCXCL16), MMP-2 (Invitrogen, Human MMP-2 ELISA Kit, CN: KHC3081), and MMP-9 (Abcam, ab246539 Human MMP-9 Simple Step ELISA® Kit) were analyzed using the respective ELISA assays as stated by the manufacturers. A total volume of 100 μL of conditioned cultured media was used in ELISA assays. Absorbance was measured at 450 nm in a 96-well plate by using a Synergy HTX microplate reader.

2.2.13. Statistical analysis

Statistical analysis was performed using Graphpad Prism 8.0 Software (Prism 8™). One-way analysis of variance (One-way ANOVA), and Two-way analysis of variance (Two-way ANOVA) was used whenever appropriate. Possible outliers within each experimental condition were analyzed with a standard Q-Test. NMR exometabolomics results statistical significance was assessed via the Mann-Whitney *U* test (non-parametric). Statistical differences were indicated as *$p < 0.05$, **$p < 0.01$ and ***$p < 0.001$. Unless otherwise indicated, $p < 0.05$ was considered statistically significant in all samples.

3. Results and discussion

The breast cancer TME is increasingly recognized to play a pivotal role in disease progression and acquisition of multi-drug resistance. Apart from the malignant and stromal cellular components of the tumor niche, the ECM surrounding the TME also plays a supporting role in cancer development, metastasis, and can act as a protective barrier to chemotherapeutics diffusion [54]. Recapitulating human TME hall- marks in *in vitro* solid tumor models may unlock the fabrication of next-generation testing platforms with an improved cross-correlation between preclinical drug screening data and the *in vivo* scenario. So far, the integration of tissue-derived dECM scaffolds in the assembly of cancer-stroma solid tumor spheroids in suspension has yet to be demonstrated. Introducing pre-existing ECM in the initial phase of spheroids assembly is key to mimic ECM natural presence during disease onset and progression, we thus hypothesize that its inclusion in 3D models will trigger important biological responses. Therefore, to tackle spheroids lack of pre-existing ECM, we established an innovative methodology based on tissue-derived decellularized ECM (dECM) microfibrillar fragments for the assembly of breast cancer spheroids comprising malignant and stromal cells. This straightforward bottom-up bioengineering method enabled the recapitulation of fundamental ECM/cellular tumor building blocks mimicking key hallmarks of native tumors in an

easy-to-reproduce methodology.

3.1.Porcine mammary adipose tissue decellularization and characterization

To better mimic the breast tissue-specific ECM we processed mammary adipose tissue into decellularized microfibrillar fragments that recapitulate the microstructural and biochemical cues sensed by cells *in vivo* [55]. For mammary adipose tissue decellularization cells and associated genomic material was removed by using a low concentration of Triton X-100 in combination with ammonium hydroxide. Non-ionic Triton X-100 detergent was selected for breast adipose tissues decellularization due to its recognized efficacy for tissues delipidation, in comparison to its ionic counterparts [56].

Fluorescence microscopy analysis of DAPI labelled dECM indicated an effective removal of cellular components and DNA (Fig. 1 C1 and C2). This analysis was complemented by fluorescence quantification of DNA content in processed dECM samples. DNA quantification data which further corroborated the efficacy of the implemented decellularization protocol in depleting genetic material with less than 50 ng of DNA being detected (Fig. 1 D).

± Quantification of total collagen content in processed dECM revealed a relative increase in collagen (147.90 ± 15.19%) in decellularized tissues (Fig. 1 E). A significant fraction of ECM glycosaminoglycans (GAGs, 61.83 10.40%), was also obtained. Collagen and GAGs content is in accordance with other reports that employed a similar decellularization protocol [57,58]. Chemically decellularized ECM was then freeze dried and further processed by mechanical homogenization. SEM analysis revealed a fibrillar arrangement that was maintained in unprocessed and homogenized dECM (HdECM - Fig. 1 F1 and F2). This dense fibrous network is highly typical of collagen rich structures. In addition, dECM microfiber fragments exhibited a similar mean diameter in unprocessed or homogenized fraction, however a higher number of microfibrillar fragments with diameters in the range of 2–4 μm was obtained in HdECMs (Fig. 1 G).

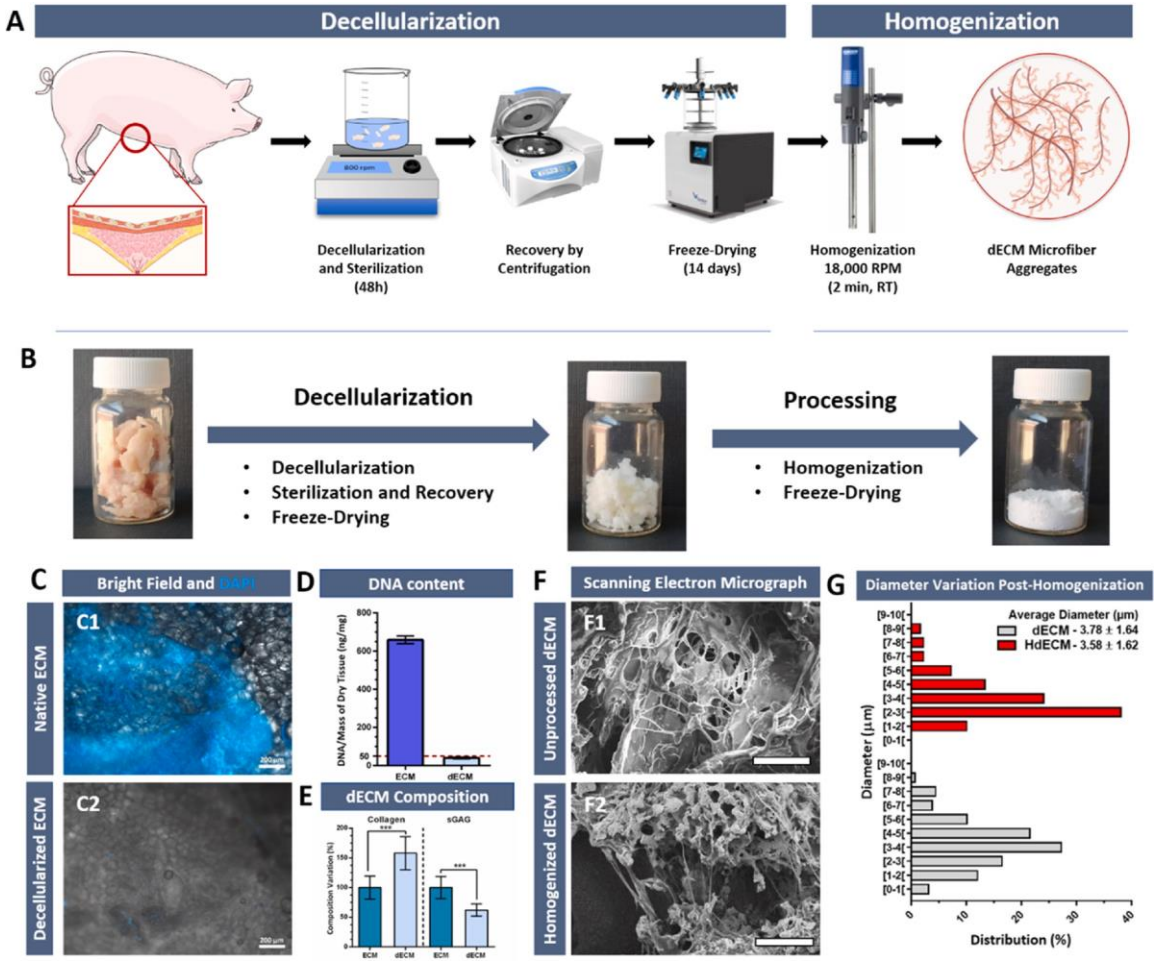

Fig. 1. Decellularization and characterization of mammary adipose tissue. (A) Schematic overview of the decellularization and recovery process. (B) Micrographs of native ECM visual appearance during the decellularization process. (C) Fluorescence microscopy analysis of DNA content in native adipose mammary tissue (C1) and in non-homogenized dECM (C2). (D) Quantitative analysis of DNA content in different ECM samples. Data is presented as mean ± s.d., $n = 3$, ***$p < 0.001$. (E) Analysis of dECM and pristine ECM collagen and sulfated GAGs. (F) SEM micrographs of freeze-dried non-homogenized dECM (F1) and homogenized dECM microfibrillar fragments (F2). (G) Analysis of dECM microfibrils diameter before, and post-homogenization (HdECM). (C – Scalebars = 200 µm; F – Scalebars = 50 µm).

3.2.*dECM-Spheroids assembly*

3D Tumor spheroid models provide a valuable platform for recapitulating key tumor hallmarks, supporting the appearance of disease relevant cellular phenotypes [59]. However, conventional spheroids models fail in recapitulating ECM composition, and pre-existing cell-ECM interactions during spheroids aggregation. Aiming to address this shortcoming, and at the same time provide a bioderived supporting matrix in which cancer and stromal cells could establish a solid tumor, we

optimized the development of dECM-enriched spherical breast cancer models.

× In all assays scaffold-free spheroids were established via the liquid overlay technique. To promote the assembly of cohesive spheroids, cells were seeded and centrifuged in ultra-low adhesion (ULA) multi-well plates (Fig. 2 A). By using this an optimized cell seeding density (30×10^3 cells/well) and a centrifugation step, scaffold-free and dECM-Spheroid formation was efficiently and reproducibly achieved.

In triple-negative breast cancer stromal invasion and activation is typically associated with worsened clinical outcomes. Histological findings highlight the tumor–stroma ratio in the primary tumor of early triple-negative breast cancer patients as an important prognostic factor [60]. Stroma-rich tumors (>50% intra-tumor stroma) tend to present decreased therapeutical response, which conjugated with increased immune evasion plays a crucial role in tumor progression [61]. Aiming to better mimic the cellular composition of metastatic breast cancer microenvironment we co-cultured triple negative breast cancer cells (MDA-MB-231) and human derived dermal fibroblasts (HF) in a 1:2 ratio, as also previously established in other reports [49]. An analysis of these heterotypic spheroids revealed that fibroblasts combination with MDA-MB-231 breast cancer cells leads to slightly increased spheroid area in comparison to their monotypic counterparts. Moreover, heterotypic spheroids demonstrated a quicker contraction rate at the initial stages of aggregation, presenting denser microtumors at 24 h, in com- parison to their monotypic counterparts (Fig. 2 C, D). All scaffold-free spheroids exhibited circularity/morphology and reproducible diameters (~350–550 μm) (Fig. 2 E, F).

Regarding the generation of ECM enriched spheroids, we propose a modified liquid overlay/centrifugation protocol which assures the formation of dECM-cell agglomerates and promotes the establishment of morphologically controlled 3D microtissues in ULA plates. In addition to this optimized protocol, we also investigated the influence of the initial amount of matrix per spheroid in the overall morphology of *in vitro* generated microtumors (Fig. 2 B, C). For this, monotypic, and hetero- typic spheroids were incubated in ULA plates containing different dECM pelleted fractions (Supplementary Fig. S1). The inclusion of 50–100 μg of dECM per well generated more variable microtumors, particularly in heterotypic models at early time-points (Fig. 2C), with multiple spheroids occasionally being obtained. The inclusion of 25 μg of breast matrix per well lead to the establishment of dECM-Spheroids with reproducible morphology and circularity in both monotypic and heterotypic conditions. dECM-Spheroids closely mimicked scaffold-free microtumors circularity and presented an increased size (Fig. 2 D, E). Along time scaffold-free heterotypic spheroids exhibited a slower contraction rate (~7.3 μm/day) in comparison to that of dECM-Spheroid counterparts (~10.3 μm/day) along the 14 days of *in vitro* maturation (Fig. 2 F). Therefore, monotypic and heterotypic dECM (25 μg)-Spheroids were used for subsequent assays.

These results demonstrate the successful implementation of the proposed methodology for assembling dECM-Spheroid models. More importantly, the ease of handling, the low labor-intensive procedure and the use of freeze dried dECM that can be viewed as an off-the-shelf element, all account for the high translatability of these models toward large HTS platforms.

In vivo solid tumor masses are characterized by restrictions in the diffusion of nutrients and oxygen, promoting altered metabolic profiles [62], and hypoxia [63], that culminate with the appearance of necrotic regions. The establishment of these altered microenvironments within tumors volume has been found to contribute to altered phenotypes and appearance of cancer/stromal cells sub-populations [64]. To analyze if such necrotic regions were formed in ECM-Spheroids Live/Dead assays were performed. Microtumors fluorescence microscopy analysis revealed that necrotic regions were visible at day 7, in all spheroid models, independently of culture conditions (Fig. 3 A and B). Interestingly, spheroids enriched with dECM exhibited higher intensity of PI signal assigned to necrotic cells in both monotypic and heterotypic models, at day 7 (Fig. 3 A 10–12, B9-10), suggesting that matrix inclusion influences the establishment of this important hallmark at early stages of spheroids development *in vitro* (Fig. 3). Furthermore, seeking to quantitatively analyze how matrix inclusion affected cellular viability and overall metabolic response ATP-based viability assays were per- formed. In comparison to scaffold-free spheroids, ATP-measurement based viability assays showed that dECM inclusion leads to a slight decrease in total ATP (Fig. 3C), particularly noticeable in heterotypic cultures. Moreover, this increase was observed in both dECM-Spheroids comprised by metastatic breast cancer cells and cancer-stromal co-cultures and suggests that alike necrotic-core formation, also cell viability/metabolic activity, is influenced at early stages by dECM inclusion (Fig. 3). Given proven biocompatible nature of utilized dECM [44,55, 65], and the fact that no adverse effects are observable in cell viability assays using monoculture spheroids, we hypothesize that these findings can be the end result of cell-ECM interactions favoring spheroid com- paction/density in the core. Moreover, this data can be also derived from the added effect of fibroblasts *de novo* ECM deposition that is reported to occur in culture along time [66]. Both these parameters can contribute to decreased nutrients uptake and oxygen deprivation, thus promoting necrotic core formation.

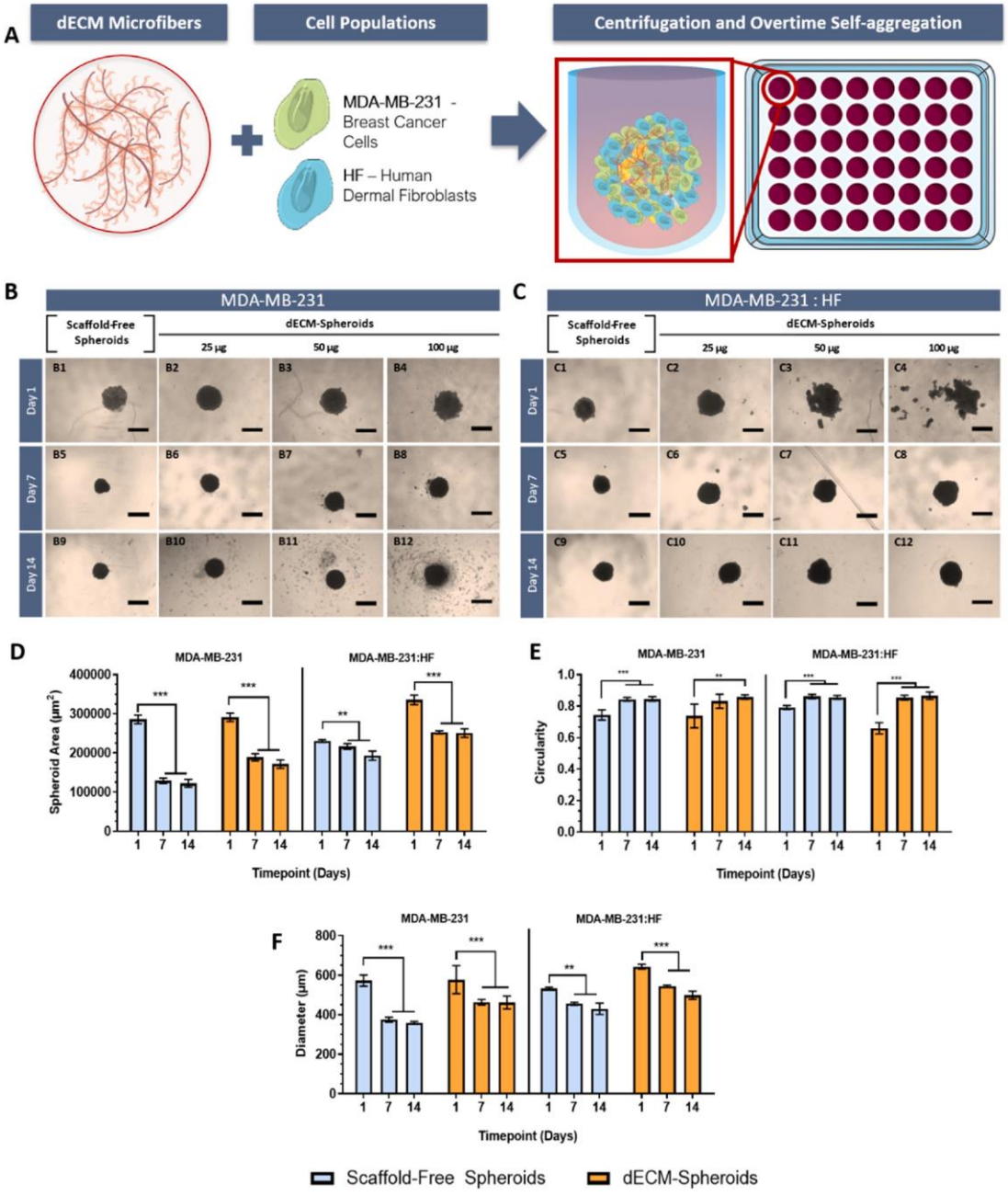

Fig. 2. Optimization of dECM-Spheroids assembly. (A) Schematic overview of the methodology optimized for establishing biomimetic microtumors. (B and C) Optical contrast micrographs of monotypic and heterotypic 3D microtissues self-assembly along time (day 1–14). Scalebars = 500 µm. (D) Spheroid's area variation, (E) circularity analysis, and (F) diameter morphological analysis of optimized 25 µg/dECM-Spheroid and scaffold-free spheroid models. All data was quantified through ImageJ algorithms. Data is presented as mean ± s.d., $n = 6$ spheroids, *$p < 0.05$, **$p < 0.01$, ***$p < 0.001$.

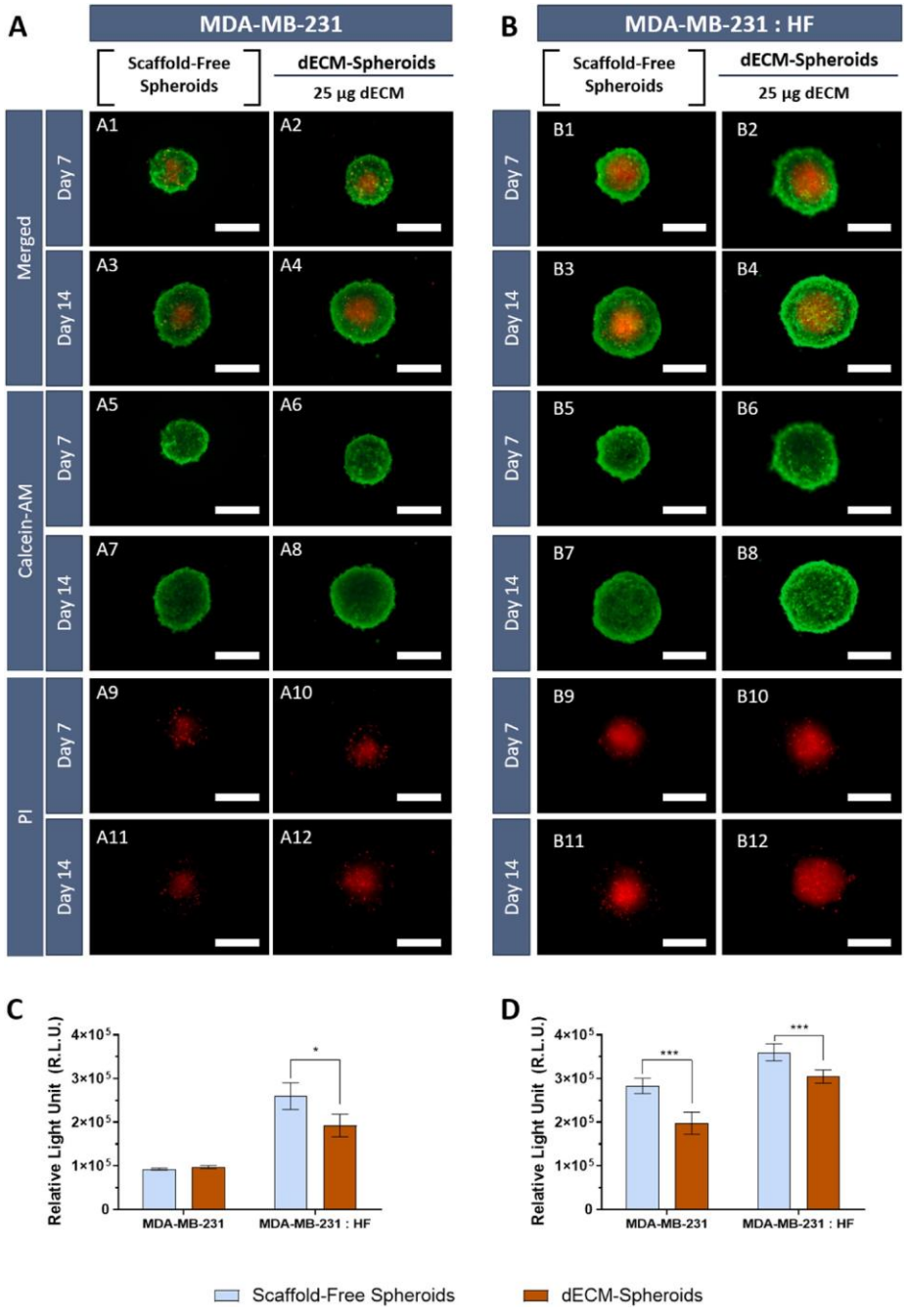

Fig. 3. dECM-Spheroids cell viability and metabolic activity characterization. Monotypic models comprised by MDA-MB-231 cancer cells and heterotypic models comprise MDA-MB-231:HF cancer-stromal cell co- Upon establishing that including breast tissue dECM enabled the assembly of MDA-MB-231 mono and co-culture spheroids, the same procedure was attempted with MCF-7 and T47D non-metastatic breast cultures. (A and B) Live/dead analysis of monotypic and heterotypic microtumors, respectively. (Calcein-AM – Green channel, Propidium iodide – red channel). Scalebars = 400 µm. (C and D) CellTiter-Glo® 3D ATP quantification assay viability analysis of monoculture and co- culture spheroids containing different amounts of dECM at (C) 7 days, and 14 (D) days of culture. Data is represented as mean ± s.d., $n = 6$, *$p < 0.05$, ***$p < 0.001$.

Upon establishing that including breast tissue dECM enabled the assembly of MDA-MB-231 mono and co-culture spheroids, the same procedure was attempted with MCF-7 and T47D non-metastatic breast cancer cell lines in monoculture and co-culture conditions. Each of these cell lines is derived from Luminal A hormone responsive breast cancers, and therefore exhibits distinctive spheroid and ECM adhesive properties when compared to metastatic MDA-MB-231 [67–69]. The less aggressive T47D cell lines exhibited similar behavior to MDA-MB-231 cells upon dECM integration, forming cohesive spheroids in both mono- culture and co-culture conditions (Supplementary Fig. S2). Regarding MCF-7 cells, this cell line generally displays low spheroid formation efficiency, exhibiting significant budding, low-circularity and cell-cell cohesion, particularly in high cell seeding density spheroids. Cohesive MCF-7 spheroids showcasing identical spherical morphologies were only observed when fibroblasts were co-cultured with the MCF-7 cell line (Supplementary Fig. S3). Co-culture MCF-7 spheroids presented smaller, more compact, dimensions, as well as decreased variation in overall spheroid budding. Similarly to MDA-MB-231 spheroids, in MCF-7:HF models the addition of dECM generally led to the formation of denser spheroids, as showcased by optical imaging and the appearance of necrotic regions (Supplementary Fig. S4). Overall, the methodology developed herein allowed the inclusion of dECM during microtumors assembly and led to the establishment of spheroids in all tested breast cancer cell lines.

3.3. *Cell-ECM architecture of dECM-Spheroids*

To further confirm dECM integration in spherical 3D microtumors the matrix was labelled with a WGA-Alexa™ 594 probe that selectively binds to glycosaminoglycan residues. Fluorescently labelled dECM was incubated using the before described methodology for microtumors assembly. As shown in 3D reconstructed confocal microscopy micro- graphs, dECM microfibrillar fragments (red channel) were fully incorporated into the structure of both monoculture and co-culture dECM-Spheroid aggregates (Fig. 4 A4 and A8).

Having established the presence and spatial distribution of dECM within spheroids, the overall cellular population arrangement was analyzed. Solid tumors are known to have specific histological and cellular distributions, with different genomic subtypes and stages of breast cancer being characterized by distinct populational distribution [70]. As such, time-course cell tracking assays were performed with the aim of understanding if randomize or cluster-like cellular organization took place in co-culture spheroids with and without dECM (Fig. 5).

Analysis of co-cultured dECM-Spheroids cancer/stromal organization demonstrates that over the course of 7 days, cultured populations tended to randomly distribute both in dECM-Spheroids containing and their pristine spheroid counterparts (Fig. 5 B). As demonstrated through high-

resolution CLSM micrographs clustering of both cancer and stromal populations into non-uniform agglomerates and randomly distributed cells within both models was observable. Triple-negative breast cancer naturally showcases stromal/cancer cell clusters with semi-defined borders in which direct cell-cell interactions between cancer, stromal and immune cells are found to be highly recurrent [71,72]. Following the characterization of dECM-Spheroids size/shape, necrotic core establishment, cell viability, and spatiotemporal distribution of cancer cells and fibroblasts in co-culture models, their utility to serve as a living platform for studying metastatic breast cancer cells invasion *in vitro* was investigated.

3.4.*Invasion assays*

During tumor progression metastatic breast cancer cells and their associated stromal cells (e.g., fibroblasts, macrophages, etc.) establish an intricate cross-talk with the supporting ECM which stimulates cancer cells motility [73,74]. To investigate feasibility of triple dECM-3D cancer-stroma models for recapitulating cells invasion *in vitro*, we embedded the optimized spheroids in Matrigel™ hydrogels that mimicked tumor surrounding tissues (Fig. 6). Matrigel represents a complex mix of growth-factors and ECM proteins derived from basement membrane extracts of Engelbreth-Holm-Swarm (EHS) murine sarcoma. Given its rich growth-factor composition and low-stiffness, Matrigel™ is generally selected as a scaffolding hydrogel for invasion and spheroid sprouting assays. Fluorescence microscopy analysis of 3D microtumor invasion into Matrigel™ revealed that the triple component dECM-Spheroid models exhibit an invasive phenotype, a feature of metastatic triple negative breast cancers. Heterotypic dECM-Spheroids show a slightly reduced invasion distance in comparison to their counterparts, particularly at 7 days post-embedding in Matrigel™ (Fig. 6 B and C), suggesting that dECM inclusion may play a role in disease progression/invasion along time, as also discussed in other studies [75–77]. Establishing a direct correlation with the complex native microenvironment of breast cancer [78], given the nature of the non-tumoral dECM included in the model, the obtained model might be better suited to represent the early stages of surrounding tissue invasion [55] rather than fully aligned fibronectin and collagen I, III and IV rich malignant tumor-ECM [76,79]. Importantly assuring the development of co-culture dECM-Spheroid models with well-defined and reproducible morphology as described herein is key for obtaining robust data from invasion assays, since including microtumors with highly variable morphology will add a significant unpredictability to sprouting/invasion analysis.

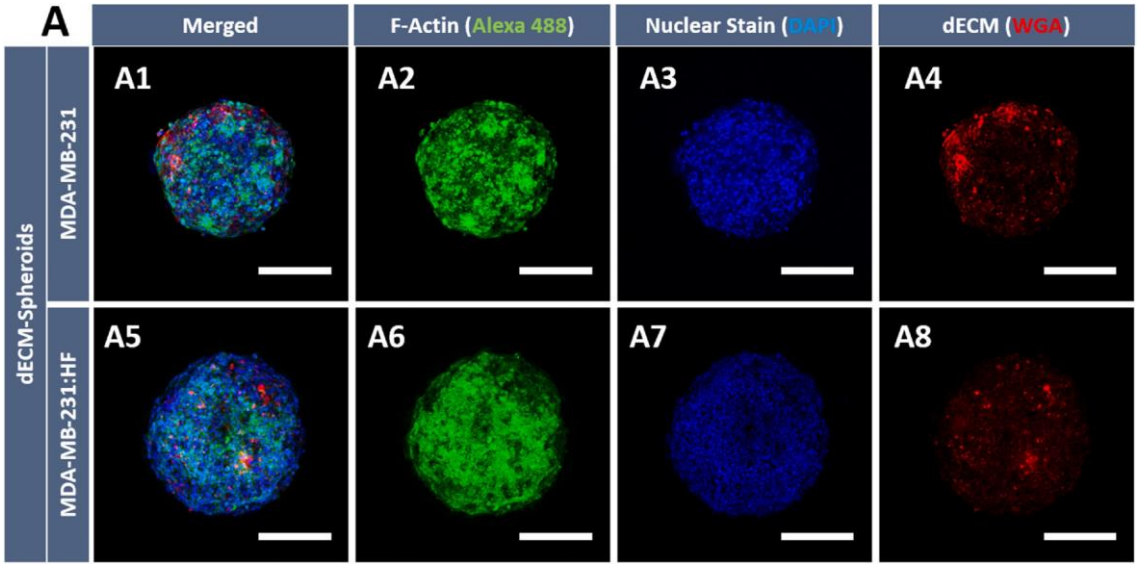

Fig. 4. Confocal microscopy analysis of dECM-Spheroids. (A) Confocal fluorescence microscopy analysis of monotypic (A1-A4) and heterotypic (A5-A8) spheroids enriched with WGA-Alexa™ 594 labelled dECM (red channel) at day 7, (DAPI labelled cell nucleus – Blue channel, Phalloidin-FITC labelled actin filaments – Green channel). Scalebars = 200 μm.

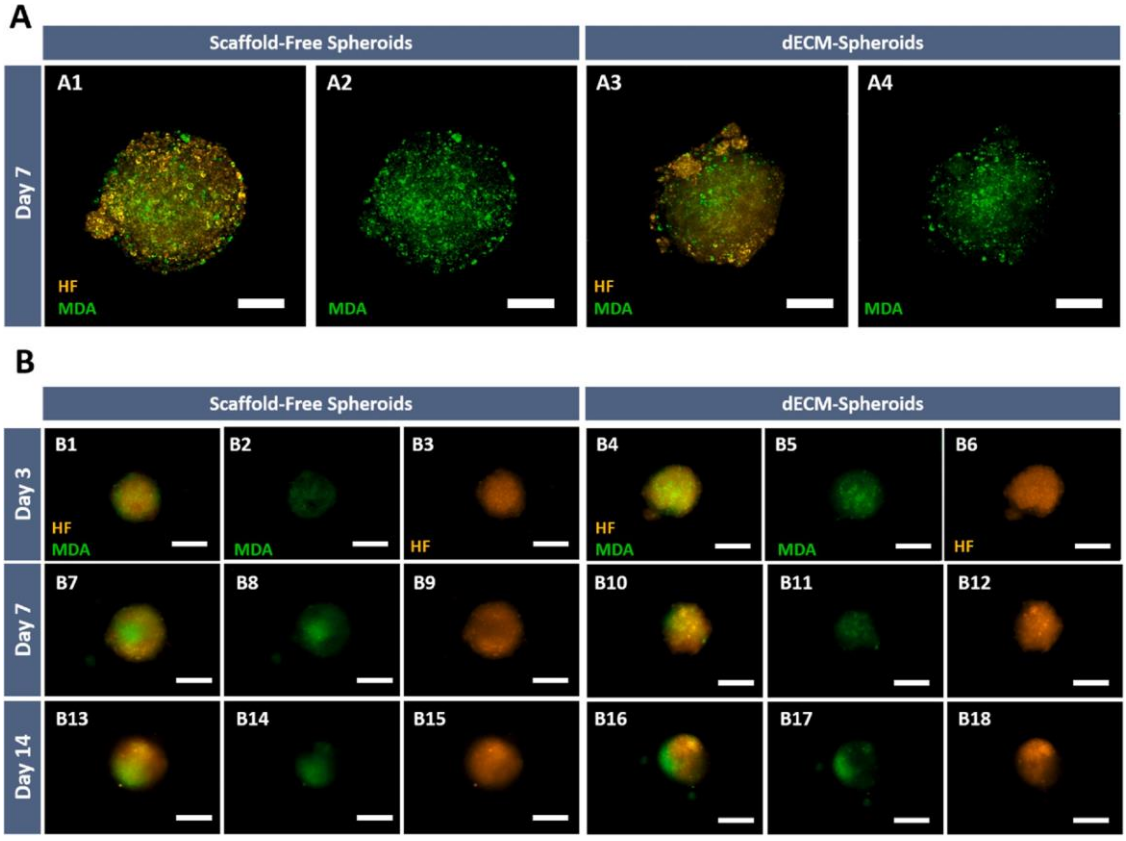

Fig. 5. (A) Confocal microscopy analysis of cellular organization in co-culture spheroids with and without dECM at day 7. MDA-MB-231 cells were labelled with DiO (Green), and HF with

DiI (Orange). Scalebars = 500 μm (B) Widefield fluorescence micrographs of optimized co-culture spheroids labelled with different cell tracking dyes. Scalebars = 250 μm. (For interpretation of the references to color in this figure legend, the reader is referred to the Web version of this article.)

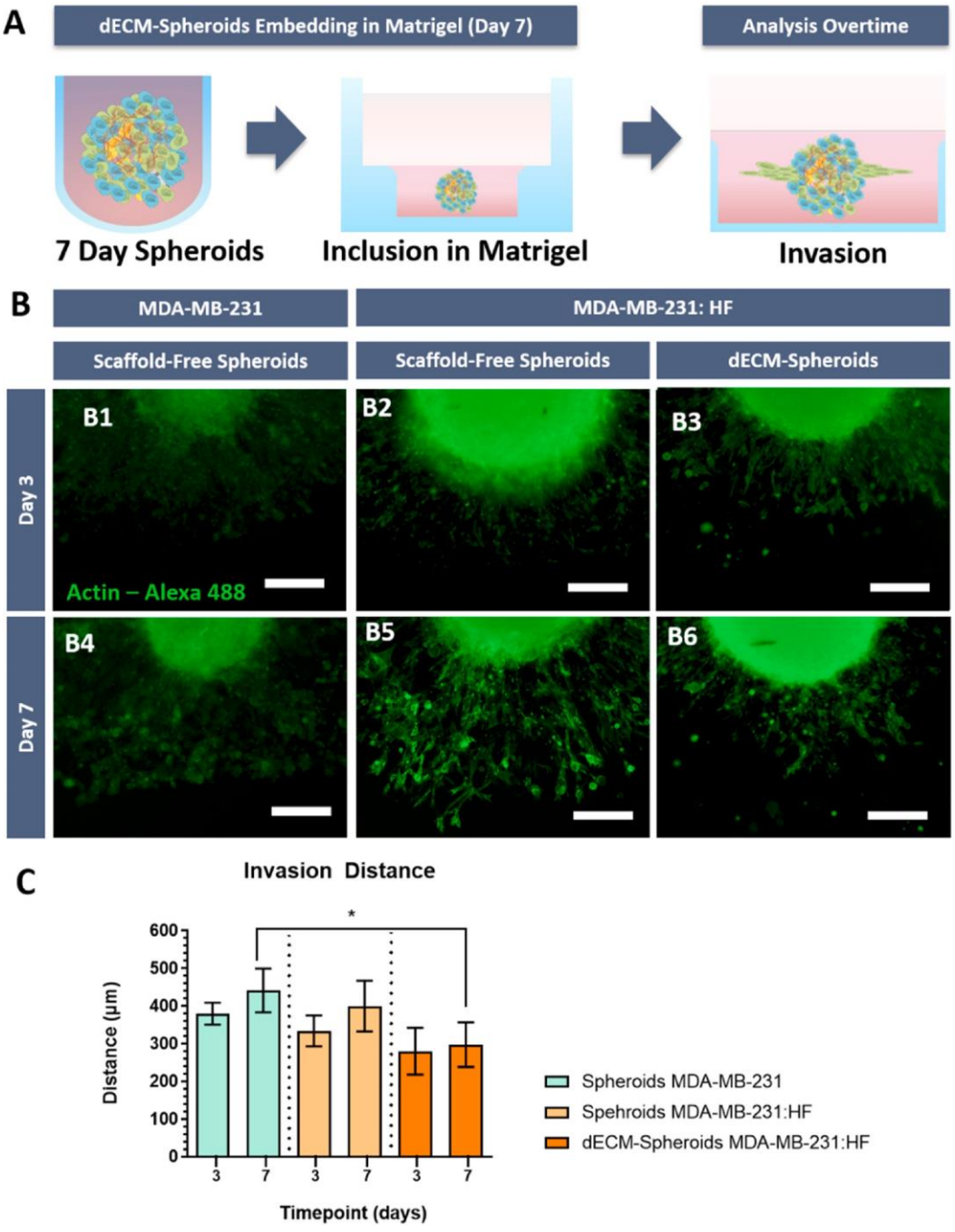

Fig. 6. dECM-Spheroids invasion analysis. (A) Schematics of invasion assays comprising monotypic and heterotypic dECM-Spheroids. (B) Fluorescence microscopy images of cells migration from different spheroid models encapsulated in Matrigel™ hydrogels. (Green channel- Phalloidin-FITC) Scalebars = 200 μm. (C) Radial invasion distance analysis of

different spheroid *in vitro* models formed at, 3 and 7 days, post embedding in Matrigel™ hydrogels. Data is presented as mean ± s.d., $n = 3$, *$p < 0.05$.

3.5.*dECM-spheroids characterization*

Seeking to better investigate the influence of including dECM fragments in microtumors physiology, the release of key soluble biomarkers was evaluated through ELISA-based analysis of matured spheroids culture media. To this end, key matrix metalloproteinases (MMPs) MMP-2 and MMP-9 [80], as well as key breast cancer biomarkers known to act as pro-tumoral, immunoregulatory and pro-angiogenic factors namely Transforming growth factor-β1 (TGF-β1) [81], and CXCL16 [82] were screened (Fig. 7). The expression of MMPs in breast cancer has been significantly correlated with basement membrane degradation and tumor-ECM remodeling, with MMP-2, MMP-7, MMP-9 and MMP-14 demonstrating leading roles in the degradation of surrounding tissues. Specifically, the ratios MMP-2 to MMP-9 levels in breast cancer microenvironments have been directly correlated with lymph node metastasis and malignancy [80,83]. Analysis of MMPs concentration overtime in co-culture dECM-Spheroids and non-dECM co-culture spheroids indicated that matrix containing spheroids generally express higher levels of MMP-2. Previous reports have demonstrated that breast cancer MMPs levels in the TME are secreted by both cancer cells and associated stromal cells and are dependent on malignancy and tumor stage [80,84]. Interestingly, in both monoculture and co-culture settings, the addition of dECM appears to promote MMP-2 secretion. Conversely, a low level of MMP-2 in patients' serum is linked to favorable prognosis in patients with triple-negative breast cancer [85].

TGF-β1 and CXCL16 are recognized as crucial biomarkers of breast cancer malignancy [81,82,86]. In the context of triple-negative breast cancer TGF-β1 has been extensively connected with context-specific inhibition or stimulation of ERK1/2 or Akt pathways stimulation [81,87]. TGF-β isoforms have the ability to regulate the expression of ECM proteins, and to stimulate the production of protease inhibitors that prevent enzymatic breakdown of the ECM in mesenchymal-like cells [12,88]. Also, TGF-β1 is a ell-recognized mediator of stromal-cancer crosstalk in the context of epithelial to mesenchymal transition, as well as breast cancer cells proliferation and survival [89,90]. Including breast tissue matrix at the early stages lead to a marked increase in TGF-β1 levels in both monotypic and heterotypic dECM-spheroids when compared to their standard scaffold-free spheroid counterparts. The increased secretion of TGF-β1, also generally observed *in vivo*, may result from the direct interactions established by cultured cells and dECM [91]. Importantly, this further corroborates that matrix inclusion in 3D models during their assembly influences their physiology toward a more physiomimetic phenotype when compared to standard spheroids.

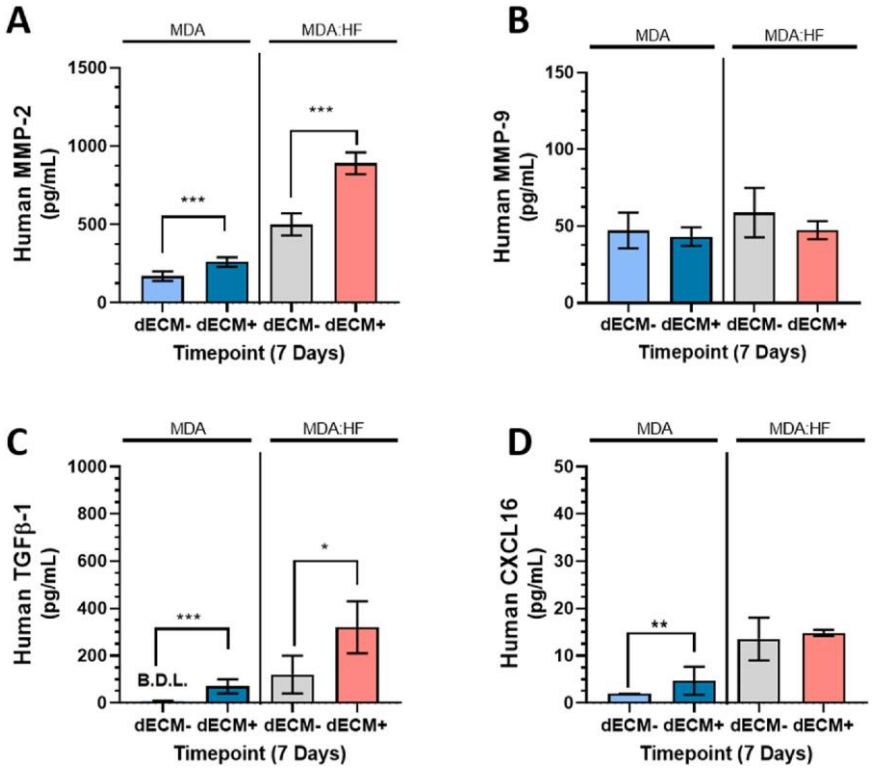

Fig. 7. The levels of secreted key matrix metalloproteinases (A) MMP-2, (B) MMP-9, and anti-inflammatory and angiogenic (C) TGF-β1, and (D) CXCL16 tumor- associated factors were measured using ELISA assays performed on supernatants prepared from optimized dECM-Spheroids and control spheroids. B.D.L. - Bellow detection limit. Data is represented as mean ± s.d., $n = 3$, *$p < 0.05$, **$p < 0.01$, ***$p < 0.001$.

Another interesting player involved in breast cancer, is the CXCL16/ CXCR6 chemokine axis, which can stabilize F-actin cytoskeleton in breast cancer cells and may play a role in invasion/metastasis process [82]. Furthermore, CXCL16 has been shown to interact with NF-kβ pathways through means of c-Rel, p105, and Rel-B cascade, playing a crucial role in for example in lung cancer cell invasion [92]. Analysis of CXCL16 expression levels revealed that, this chemokine was significantly secreted by heterotypic spheroids and specifically by dECM-enriched spheroids. We hypothesize that CXCL16 stimulation of NF-κB pathway may be partially contributing to an increase in MMP-2 in monotypic spheroids [92,93]. Overall, these biomolecular insights, highlight the importance of representing both cellular and matrix components of the TME in *in vitro* models so as to better recapitulate key physiological traits of human neoplasia.

3.6.*Cytotoxic drug screening*

Drug-screening assays were performed to evaluate the importance of the cell-cell and cell-ECM tumor microenvironment interactions on 3D *in vitro* microtumors therapeutic response. The contributions of monoculture, co-culture and dECM-enriched spheroids to overall therapeutic resistance were analyzed through drug-screening assays of three chemotherapeutics - cisplatin, gemcitabine and palbociclib [94]. With this aim, the administration of each compound was performed in 3D microtumors cultured for 7 days. Our findings indicate that dECM-3D co-culture and monoculture spheroids tend to present a slightly increased resistance to cisplatin at the higher dose (50 μM, Fig. 8 A and B), in comparison to their non-dECM counterparts. The inclusion of fibroblasts in all models lead to an increase in overall cell survival to cisplatin, in gemcitabine and palbociclib significant differences correlated with fibroblasts inclusion were observable on the highest administered dose (Fig. 8 B and C), indicating the importance of also recapitulating the inclusion of stromal cells in 3D microtumors. Within this context, the future use of non-activated breast cancer specific CAFs may provide further physiomimetic potential. The optimized dECM-Spheroid methodology is highly modular and enables an easy inclusion of different cellular populations being envisioned that the inclusion of such populations is feasible in the foreseeable future.

The TNBC tumor microenvironment is particularly recognized by comprising an activated stromal population that in combination with cancer cells promotes the establishment of a pro-tumoral microenvironment [95,96]. Moreover, in triple-negative breast cancer the inherent cross-talk established between cancer cells and associated stromal cells has been found to upregulate the release of pro-tumoral factors, that can contribute drug resistance, such as that directed to platinum-based compounds (e.g., cisplatin) [97,98]. In this context the increased expression of immune-regulatory and pro-tumoral factors as observed with TGF-β1 and CXCL16 in dECM-Spheroids might also contribute to the observed increase in cell survival in cisplatin treated monoculture and co-culture dECM-Spheroids. Specifically, both TGF-β1 and CXCL16 are recognized to activate the PI3K/Akt/mTOR pathway, which is involved in cisplatin resistance in both breast and lung cancers [99,100].

To better understand how the inclusion of dECM and stromal com- ponents affected triple-negative breast cancer cells response to cisplatin treatment, a reporter cell line MDA-MB-231 expressing luciferase and GFP was used to quantify cancer cell specific chemotoxicity. Cisplatin cytotoxicity screening in co-culture spheroids containing MDA-MB-231- Luc-GFP revealed that dECM inclusion significantly impacted cancer cells resistance to cisplatin at the highest concentrations (Fig. 8). Moreover, gemcitabine and palbociclib cytotoxicity assays revealed statistically significant increases in cancer cells specific resistance in heterotypic dECM-Spheroid models.

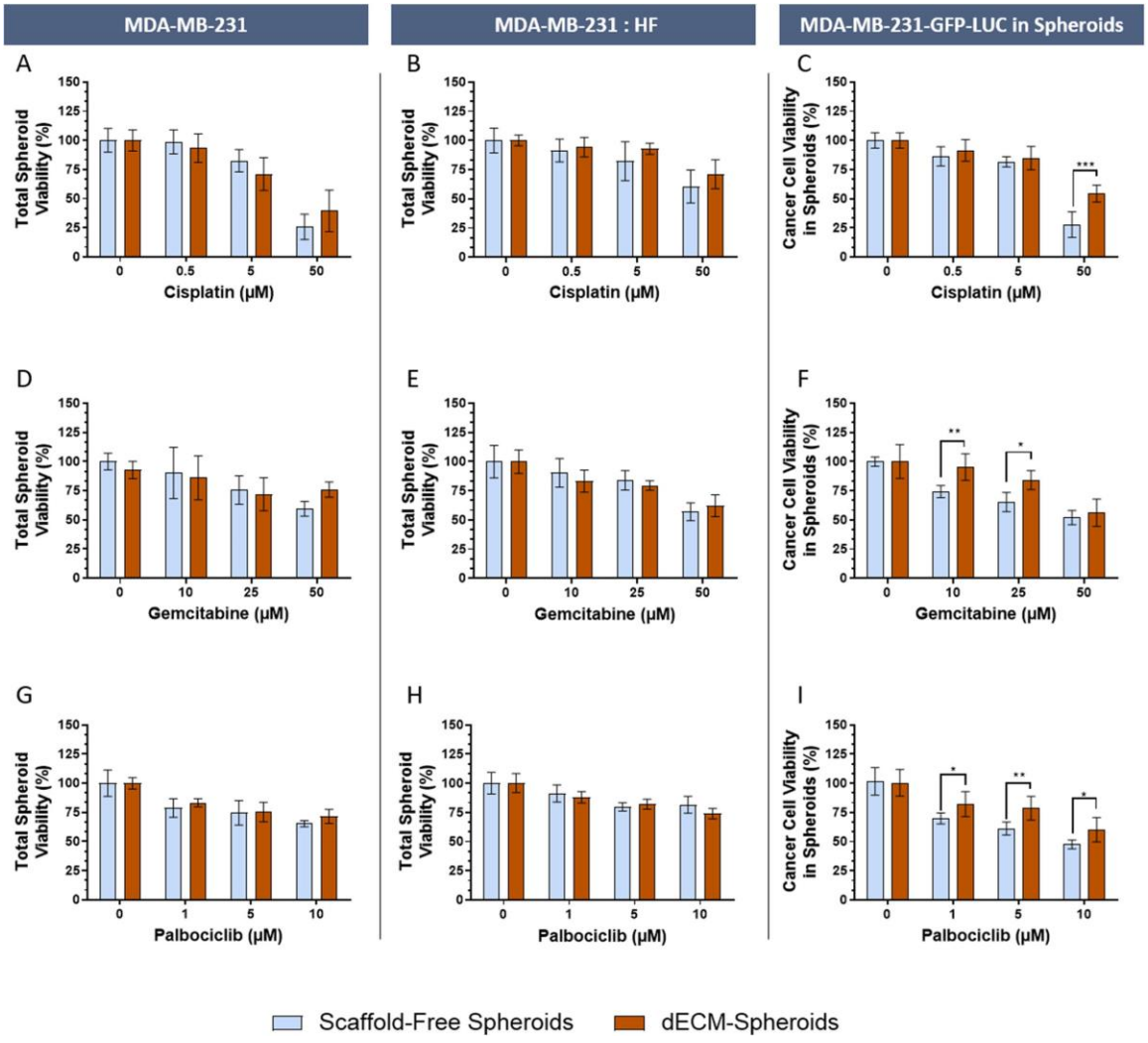

Fig. 8. Drug screening in breast cancer spheroids. (A, D and G) MDA-MB-231 monotypic spheroid viability represented on the left column, and (B, E and H) MDA- MB-231:HF in a 1:2 ratio heterotypic spheroid total viability on the center column, and (C, F and I) cancer cell specific viability in heterotypic spheroids. (A and B) Cisplatin, (D and E) Gemcitabine, and (G and H) Palbociclib chemotoxicity analysis by using CellTiter-Glo® 3D ATP quantification assay. (C) Cisplatin, (F) Gemcitabine and (I) Palbociclib chemotoxicity analysis in MDA-MB-231-Luc-GFP cell line, performed at 7 days in heterotypic spheroids assembled with and without dECM. Data is presented as mean ± s.d., $n = 6$, *p < 0.05, **p < 0.01, ***p < 0.001.

These results raise important questions regarding the cell-cell and cell-ECM mechanisms tacking place under dECM-Spheroids culture conditions in comparison to control co-culture spheroids presenting an interesting starting point for further studies. Amongst the distinct mechanisms through which the TME and cancer cells interactions pro- mote cancer resistance to therapy is the acquisition and promotion of altered epigenetic, biochemical and metabolic regulatory communications that can ultimately lead to the acquisition or promotion of resistance mechanisms in cancer cells. Hence

aiming to further characterize the developed spheroidal dECM-3D co-culture spheroids metabolic energetics of these *in vitro* models was investigated by using proton NMR exometabolomics since this non-invasive technique has shown to be a viable indicator of cellular processes that are activated in human tumors as we and others have demonstrated [101,102].

3.7.*Exometabolomics profiling of dECM-Spheroid models*

The role of tumor microenvironment populations in the regulation of cancer cells metabolic activity is increasingly seen as a crucial standing point for the development of more effective and patient-targeted therapies [102]. In order to analyze the metabolic activity of dECM-Spheroids in comparison to their mono and co-culture counter- parts, we performed a ^{1}H NMR exometabolomic profiling (Fig. 9).

Exometabolomics analysis indicated that the metabolic profile of co- culture dECM-Spheroids, expressed by metabolite consumption and excretion patterns (Fig. 9B), mirrored the one commonly associated with the native breast cancer microenvironment and its high proliferative, invasive and remodeling capacity [103,104]. Importantly, fibroblasts inclusion in both dECM and non-dECM models led to visible changes in their exometabolomic profiles compared to monotypic breast cancer counterparts, as clearly shown by multivariate analysis (Fig. 9A). Such findings emphasize the metabolic impact of stromal cells inclusion on metastatic breast cancer 3D models. In fact, fibroblasts have been recognized to play a key role in breast cancer metabolism since these stromal cells actively secrete L-lactate and promote metabolic shifts in the tumor microenvironment [105]. Globally, cells actively consumed pyruvate, glucose, fructose and several amino acids, while excreting formate, short chain fatty acids (arising from branch chain amino acids metabolism), alanine and lactate. This profile is consistent with the high glycolytic activity recognized to occur in human tumors [106], and has been previously identified as a hallmark of breast cancer via metabolomics profiling of human tumor tissue samples [107].

Correlating all the obtained data, it is clear that inclusion of both fibroblasts and dECM influences breast cancer spheroids metabolism in different modes. Overall, these results further indicate that ECM-cancer- stromal triple component models recapitulate key tumor metabolic features expanding their potential as *in vitro* models.

Such omic-based characterization is highly valuable from a bioengineering and medical perspective since it not only contributes to shed light on a major hallmark of human tumors, i.e., tumor metabolism, but also serves to possibly identify the feasibility of using co-culture dECM- Spheroid models as tools for screening candidate therapies that are specifically targeted to key tumor metabolic

signatures. In fact, considering that the field of cancer metabolism and the screening of metabolism targeted therapeutics is rapidly evolving [108–110], the existence of metabolically characterized 3D *in vitro* platforms that can be used to screen targeted therapeutics may aid in accelerating the discovery/preclinical validation of metabolism targeted precision cancer therapies in the foreseeable future.

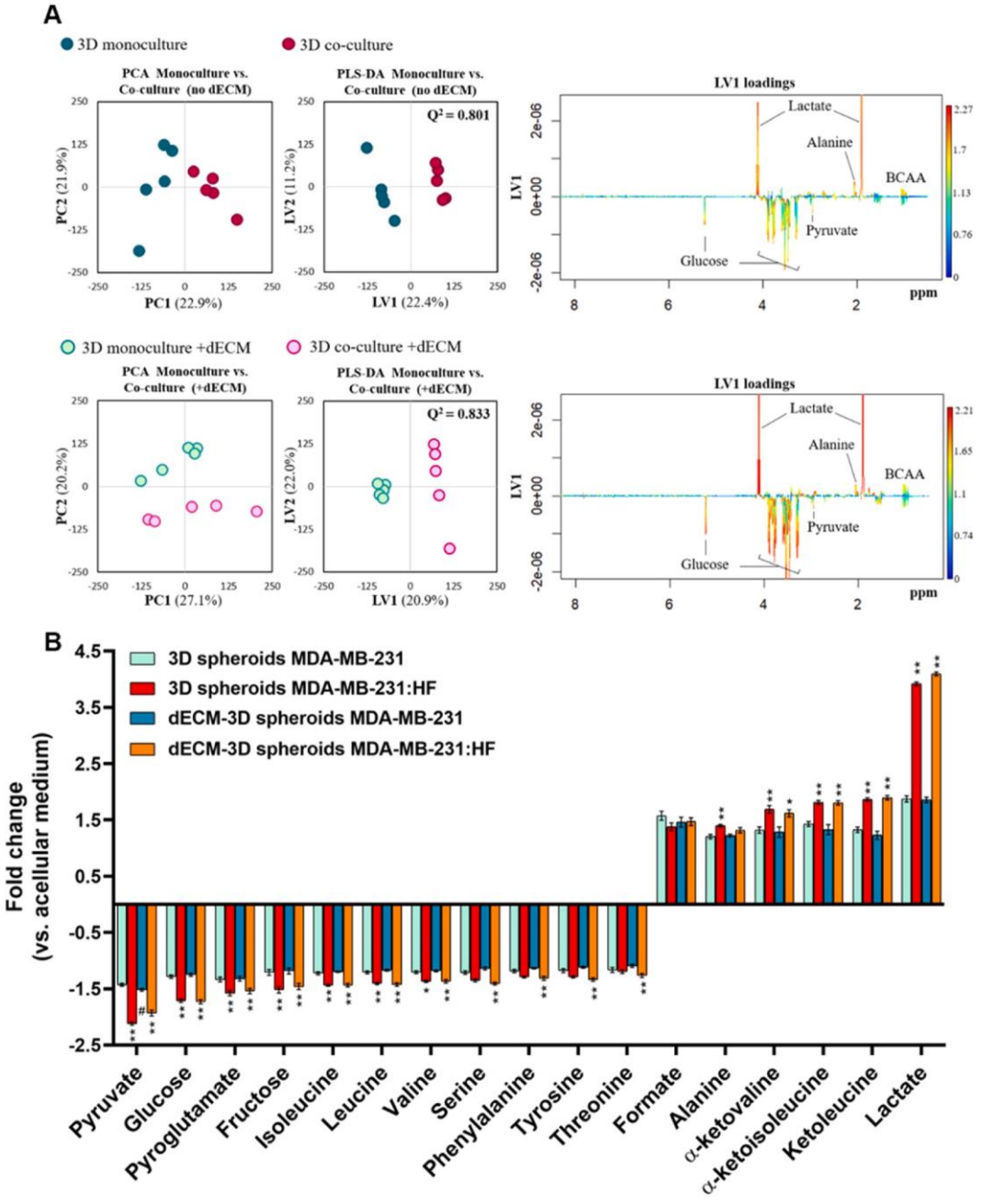

Fig. 9. Exometabolomics analysis of 3D breast cancer spheroid *in vitro* models. (A) PCA scores scatter plots (left), PLS-DA scores scatter plots (middle) and LV1 loadings plots (right) obtained

through multivariate analysis of ^{1}H NMR spectral profiles of culture medium supernatants; Positive loadings correspond to metabolites increased in co-culture-derived media (positive LV1 scores) and negative loadings to metabolites more abundant in monoculture-derived media (negative LV1 scores); (B) Main metabolites consumed (negative fold change) and excreted (positive fold change) by monotypic and heterotypic 3D models. Co-culture vs monoculture: *p < 0.05, **p < 0.01, dECM vs. no dECM: # <0.05.

4. Conclusions

Currently, scaffold-free spherical 3D tumor models have been able to effectively provide a more *in vivo*-like environment in a laboratory setting. However, most spheroid models lack the inclusion of extracellular matrix during cell aggregation stages. Herein, we were able to establish an innovative experimental methodology for integrating microfibrillar dECM fragments in mono and co-cultured spheroids assembly process, further contributing for recapitulating key cellular and matrix components of the tumor microenvironment. We were able to optimize cells-matrix self-assembly into morphologically defined 3D microtumors *in vitro*, in both non-metastatic and metastatic breast cancer cell lines, thus providing significant advances over re-cellularized dECM scaffolds or dECM cell laden hydrogels, that include randomly distributed cancer cells and multi-aggregates with variable morphologies and features.

Collectively, our findings evidence that dECM inclusion promoted spheroids compaction in most of tested non-triple-negative lineages, and recapitulation of key breast tumors hallmarks specifically in the context of heterotypic spheroids, *i.e.*, containing fibroblasts. Particularly, MDA- MB-231, co-culture spheroids including fibroblasts and dECM exhibited an increased expression of key biomarkers, and metabolomic that translated in differences to cisplatin, gemcitabine and palbociclib cancer-cell specific response. The different observations obtained in dECM-Spheroid co-culture models corroborates the need to further analyze the influence of both cell-cell and cell-ECM interactions on metastatic breast cancer models. Furthermore, the herein proposed approach provides an easy-to-perform and reproducible methodology which enables the development of more TME-ECM physiomimetic *in vitro* tumors models amenable for high-throughput/high-content screening, either in 96-well plate formats or others that may be suitable. We envision that the modularity of this methodology will further allow the inclusion of other tumor building blocks such as tumor associated fibroblasts, tumor associated macrophages, or other tissue- specific ECM fragments into spheroid models in the future. Moreover, the universal character of cell-ECM interactions opens new avenues for also establishing dECM-Spheroid models from patient derived xenographs or primary cells and from human tumor derived dECM, further expanding the possibility to explore patient personalized

treatments. These next-generation matrix-rich spheroids are expected to facilitate the discovery of fundamental mechanisms or new tumor biomarkers and to contribute for accelerating the preclinical anti-cancer drug screening of candidate therapeutics.

Data availability

The raw/processed data required to reproduce these findings cannot be shared at this time as the data also forms part of an ongoing study.

Declaration of competing interest

The authors declare that they have no known competing financial interests or personal relationships that could have appeared to influence the work reported in this paper.

Acknowledgements

This work was developed within the scope of the project CICECO- Aveiro Institute of Materials, UIDB/50011/2020 & UIDP/50011/2020, financed by national funds through the FCT/MEC and when appropriate co-financed by FEDER under the PT2020 Partnership Agreement. This work was also supported by the Programa Operacional Competitividade e Internacionalização (POCI), in the component FEDER, and by national funds (OE) through FCT/MCTES, in the scope of the project PANGEIA (PTDC/BTM-SAL/30503/2017). Vítor Gaspar acknowledges funding in the form of a Junior Researcher Contract under the scope of the project PANGEIA (PTDC/BTM-SAL/30503/2017). The authors acknowledge the financial support by the Portuguese Foundation for Science and Technology (FCT) through an individual Doctoral Grant (SFRH/BD/ 141718/2018, Luís Ferreira). Confocal imaging acquisition was per- formed in the LiM Facility of iBiMED, a node of PPBI (Portuguese Platform of BioImaging): POCI-01-0145-FEDER-022122. The NMR spectrometer is part of the National NMR Network (PTNMR), partially supported by Infrastructure Project Nº 022161 (co-financed by FEDER through COMPETE 2020, POCI and PORL and FCT through PIDDAC).

Appendix A. Supplementary data

Supplementary data to this article can be found online at xxx.

References

[1] S. Pradhan, J.H. Slater, Tunable hydrogels for controlling phenotypic cancer cell states

to model breast cancer dormancy and reactivation, Biomaterials 215 (2019), 119177, https://doi.org/10.1016/j.biomaterials.2019.04.022.

[2] J.A. Belgodere, C.T. King, J.B. Bursavich, M.E. Burow, E.C. Martin, J.P. Jung, Engineering breast cancer microenvironments and 3D bioprinting, Front. Bioeng. Biotechnol. 6 (2018), https://doi.org/10.3389/fbioe.2018.00066.

[3] N. Sachs, J. de Ligt, O. Kopper, E. Gogola, G. Bounova, F. Weeber, A.V. Balgobind, K. Wind, A. Gracanin, H. Begthel, J. Korving, R. van Boxtel, A.A. Duarte, D. Lelieveld, A. van Hoeck, R.F. Ernst, F. Blokzijl, I.J. Nijman, M. Hoogstraat, M. van de Ven, D.A. Egan, V. Zinzalla, J. Moll, S.F. Boj, E.E. Voest, L. Wessels, P.
J. van Diest, S. Rottenberg, R.G.J. Vries, E. Cuppen, H. Clevers, A living biobank of breast cancer organoids captures disease heterogeneity, Cell 172 (2018) 373–386, https://doi.org/10.1016/j.cell.2017.11.010, e10.

[4] M. Zanoni, F. Piccinini, C. Arienti, A. Zamagni, S. Santi, R. Polico, A. Bevilacqua, A. Tesei, 3D tumor spheroid models for in vitro therapeutic screening: a systematic approach to enhance the biological relevance of data obtained, Sci. Rep. 6 (2016) 19103, https://doi.org/10.1038/srep19103.

[5] J. Friedrich, C. Seidel, R. Ebner, L.A. Kunz-Schughart, Spheroid-based drug screen: considerations and practical approach, Nat. Protoc. 4 (2009) 309–324, https://doi.org/10.1038/nprot.2008.226.

[6] T. Rodrigues, B. Kundu, J. Silva-Correia, S.C. Kundu, J.M. Oliveira, R.L. Reis, V. M. Correlo, Emerging tumor spheroids technologies for 3D in vitro cancer modeling, Pharmacol. Ther. 184 (2018) 201–211, https://doi.org/10.1016/j. pharmthera.2017.10.018.

[7] L.P. Ferreira, V.M. Gaspar, J.F. Mano, Design of spherically structured 3D in vitro tumor models -Advances and prospects, Acta Biomater. 75 (2018) 11–34, https:// doi.org/10.1016/j.actbio.2018.05.034.

[8] M. Pal, H. Chen, B.H. Lee, J.Y.H. Lee, Y.S. Yip, N.S. Tan, L.P. Tan, Epithelial-mesenchymal transition of cancer cells using bioengineered hybrid scaffold composed of hydrogel/3D-fibrous framework, Sci. Rep. 9 (2019) 1–11, https:// doi.org/10.1038/s41598-019-45384-9.

[9] S.C. Casey, A. Amedei, K. Aquilano, A.S. Azmi, F. Benencia, D. Bhakta, A. E. Bilsland, C.S. Boosani, S. Chen, M.R. Ciriolo, S. Crawford, H. Fujii, A. G. Georgakilas, G. Guha, D. Halicka, W.G. Helferich, P. Heneberg, K. Honoki, W. N. Keith, S.P. Kerkar, S.I. Mohammed, E. Niccolai, S. Nowsheen, H.P. Vasantha Rupasinghe, A. Samadi, N. Singh, W.H. Talib, V. Venkateswaran, R.L. Whelan, X. Yang, D.W. Felsher, Cancer prevention and therapy through the modulation of the tumor microenvironment, Semin. Canc. Biol. 35 (2015) S199–S223, https:// doi.org/10.1016/j.semcancer.2015.02.007.

[10] C. Walker, E. Mojares, A. del Río Hern´andez, Role of extracellular matrix in development and cancer progression, Int. J. Mol. Sci. 19 (2018) 3028, https:// doi.org/10.3390/ijms19103028.

[11] A. Malandrino, M. Mak, R.D. Kamm, E. Moeendarbary, Complex mechanics of the heterogeneous extracellular matrix in cancer, Extrem. Mech. Lett. 21 (2018) 25–34, https://doi.org/10.1016/j.eml.2018.02.003.

[12] M. Najafi, B. Farhood, K. Mortezaee, Extracellular matrix (ECM) stiffness and degradation as cancer drivers, J. Cell. Biochem. 120 (2019) 2782–2790, https:// doi.org/10.1002/jcb.27681.

[13] P. Lu, V.M. Weaver, Z. Werb, The extracellular matrix: a dynamic niche in cancer progression, J. Cell Biol. 196 (2012) 395–406, https://doi.org/10.1083/ jcb.201102147.

[14] C.E. Chiang, Y.Q. Fang, C.T. Ho, M. Assunç˜ao, S.J. Lin, Y.C. Wang, A. Blocki, C.
C. Huang, Bioactive decellularized extracellular matrix derived from 3D stem cell spheroids under macromolecular crowding serves as a scaffold for tissue engineering, Adv. Healthc. Mater. (2021) 1–13, https://doi.org/10.1002/ adhm.202100024, 2100024.
[15] N.V. Kosheleva, Y.M. Efremov, B.S. Shavkuta, I.M. Zurina, D. Zhang, Y. Zhang, N. V. Minaev, A.A. Gorkun, S. Wei, A.A. Shpichka, I.N. Saburina, P.S. Timashev, Cell spheroid fusion: beyond liquid drops model, Sci. Rep. 10 (2020) 1–15, https:// doi.org/10.1038/s41598-020-69540-8.
[16] S. Raghavan, P. Mehta, E.N. Horst, M.R. Ward, K.R. Rowley, G. Mehta, Comparative analysis of tumor spheroid generation techniques for differential in vitro drug toxicity, Oncotarget 7 (2016) 16948–16961, https://doi.org/ 10.18632/oncotarget.7659.
[17] F. Tao, K. Sayo, K. Sugimoto, S. Aoki, N. Kojima, Development of a tunable method to generate various three-dimensional microstructures by replenishing macromolecules such as extracellular matrix components and polysaccharides, Sci. Rep. 10 (2020) 1–12, https://doi.org/10.1038/s41598-020-63621-4.
[18] B. Glimelius, B. Norling, T. Nederman, J. Carlsson, Extracellular matrices in multicellular spheroids of human glioma origin: increased incorporation of proteoglycans and fibronectin as compared to monolayer cultures, Apmis 96 (1988) 433–444, https://doi.org/10.1111/j.1699-0463.1988.tb05327.x.
[19] T. Nederman, B. Glimelius, B. Norling, J. Carlsson, U. Brunk, Demonstration of an extracellular matrix in multicellular tumor spheroids, Cancer Res. 44 (1984) 3090–3097.
[20] S. Singh, L.A. Ray, P. Shahi Thakuri, S. Tran, M.C. Konopka, G.D. Luker, H. Tavana, Organotypic breast tumor model elucidates dynamic remodeling of tumor microenvironment, Biomaterials 238 (2020), 119853, https://doi.org/ 10.1016/j.biomaterials.2020.119853.
[21] M.V. Monteiro, V.M. Gaspar, L.P. Ferreira, J.F. Mano, Hydrogel 3D in vitro tumor models for screening cell aggregation mediated drug response, Biomater. Sci. 8 (2020) 1855–1864, https://doi.org/10.1039/C9BM02075F.
[22] J. Antunes, V.M. Gaspar, L. Ferreira, M. Monteiro, R. Henrique, C. Jero´nimo, J. F. Mano, In-air production of 3D co-culture tumor spheroid hydrogels for expedited drug screening, Acta Biomater. 94 (2019) 392–409, https://doi.org/ 10.1016/j.actbio.2019.06.012.
[23] J. Plava, M. Cihova, M. Burikova, M. Matuskova, L. Kucerova, S. Miklikova, Recent advances in understanding tumor stroma-mediated chemoresistance in breast cancer, Mol. Canc. 18 (2019) 1–10, https://doi.org/10.1186/s12943-019- 0960-z.
[24] B. Lim, W.A. Woodward, X. Wang, J.M. Reuben, N.T. Ueno, Inflammatory breast cancer biology: the tumour microenvironment is key, Nat. Rev. Canc. 18 (2018) 485–499, https://doi.org/10.1038/s41568-018-0010-y.
[25] P. Aftimos, H.A. Azim, C. Sotiriou, Molecular biology of breast cancer, Mol. Pathol. Mol. Basis Hum. Dis. (2017) 569–588, https://doi.org/10.1016/B978-0- 12-802761-5.00026-2.
[26] C.K. Anders, V. Abramson, T. Tan, R. Dent, The evolution of triple-negative breast cancer: from biology to novel therapeutics, Am. Soc. Clin. Oncol. Educ. B. 36 (2016) 34–42, https://doi.org/10.14694/edbk_159135.
[27] M.B. Oliveira, J.F. Mano, High-throughput screening for integrative biomaterials design: exploring advances and new trends, Trends Biotechnol. 32 (2014) 627–636, https://doi.org/10.1016/j.tibtech.2014.09.009.

[28] Q. Yao, Y.-W.W. Zheng, Q.-H.H. Lan, L. Kou, H.-L.L. Xu, Y.-Z.Z. Zhao, Recent development and biomedical applications of decellularized extracellular matrix biomaterials, Mater. Sci. Eng. C 104 (2019), 109942, https://doi.org/10.1016/j.msec.2019.109942.

[29] L.W.L.W. Dunne, Z. Huang, W. Meng, X. Fan, N. Zhang, Q. Zhang, Z. An, Human decellularized adipose tissue scaffold as a model for breast cancer cell growth and drug treatments, Biomaterials 35 (2014) 4940–4949, https://doi.org/10.1016/j.biomaterials.2014.03.003.

[30] Q. Jin, G. Liu, S. Li, H. Yuan, Z. Yun, W. Zhang, S. Zhang, Y. Dai, Y. Ma, W. Zhang,
H. Yuan, S. Li, G. Liu, Y. Ma, Q. Jin, Y. Dai, Decellularized breast matrix as bioactive microenvironment for in vitro three-dimensional cancer culture, J. Cell. Physiol. 234 (2018) 3425–3435, https://doi.org/10.1002/jcp.26782.

[31] L.P. Ferreira, V.M. Gaspar, J.F. Mano, Decellularized extracellular matrix for bioengineering physiomimetic 3D in vitro tumor models, Trends Biotechnol. (2020) 1–18, https://doi.org/10.1016/j.tibtech.2020.04.006.

[32] N.A. Espinoza-Sa´nchez, G.K. Chimal-Ramírez, E.M. Fuentes-Panana´, Analyzing the communication between monocytes and primary breast cancer cells in an extracellular matrix extract (ECME)-based three-dimensional system, J. Vis. Exp. 2018 (2018) 1–11, https://doi.org/10.3791/56589.

[33] A.L. Wishart, S.J. Conner, J.R. Guarin, J.P. Fatherree, Y. Peng, R.A. McGinn, R. Crews, S.P. Naber, M. Hunter, A.S. Greenberg, M.J. Oudin, Decellularized extracellular matrix scaffolds identify full-length collagen VI as a driver of breast cancer cell invasion in obesity and metastasis, Sci. Adv. 6 (2020) eabc3175, https://advances.sciencemag.org/lookup/doi/10.1126/sciadv.abc3175.

[34] W. Li, X. Hu, S. Wang, Y. Xing, H. Wang, Y. Nie, T. Liu, K. Song, Multiple comparisons of three different sources of biomaterials in the application of tumor tissue engineering in vitro and in vivo, Int. J. Biol. Macromol. 130 (2019) 166–176, https://doi.org/10.1016/j.ijbiomac.2019.02.136.

[35] N.L. Springer, N.M. Iyengar, R. Bareja, A. Verma, M.S. Jochelson, D.D. Giri, X. K. Zhou, O. Elemento, A.J. Dannenberg, C. Fischbach, Obesity-associated extracellular matrix remodeling promotes a macrophage phenotype similar to tumor-associated macrophages, Am. J. Pathol. 189 (2019) 2019–2035, https://doi.org/10.1016/j.ajpath.2019.06.005.

[36] B.R. Seo, P. Bhardwaj, S. Choi, J. Gonzalez, R.C.A. Eguiluz, K. Wang, S. Mohanan, P.G. Morris, B. Du, X.K. Zhou, L.T. Vahdat, A. Verma, O. Elemento, C.A. Hudis, R. M. Williams, D. Gourdon, A.J. Dannenberg, C. Fischbach, Obesity-dependent changes in interstitial ECM mechanics promote breast tumorigenesis, Sci. Transl. Med. 7 (2015), https://doi.org/10.1126/scitranslmed.3010467.

[37] W. Li, X. Hu, S. Yang, S. Wang, C. Zhang, H. Wang, Y.Y. Cheng, Y. Wang, T. Liu,
K. Song, A novel tissue-engineered 3D tumor model for anti-cancer drug discovery, Biofabrication 11 (2018), 015004, https://doi.org/10.1088/1758- 5090/aae270.

[38] G. Liu, B. Wang, S. Li, Q. Jin, Y. Dai, Human breast cancer decellularized scaffolds promote epithelial-to-mesenchymal transitions and stemness of breast cancer cells in vitro, J. Cell. Physiol. 234 (2019) 9447–9456, https://doi.org/10.1002/ jcp.27630.

[39] K.A. Pence, D.K. Mishra, M. Thrall, B. Dave, M.P. Kim, Breast cancer cells form primary tumors on ex vivo four-dimensional lung model, J. Surg. Res. 210 (2017) 181–187, https://doi.org/10.1016/j.jss.2016.11.019.

[40] A. Gaiko-Shcherbak, G. Fabris, G. Dreissen, R. Merkel, B. Hoffmann, E. Noetzel, The acinar cage: basement membranes determine molecule exchange and mechanical stability of human breast cell acini, PLoS One 10 (2015) 1–20, https://doi.org/10.1371/journal.pone.0145174.
[41] P.A. Mollica, E.N. Booth-Creech, J.A. Reid, M. Zamponi, S.M. Sullivan, X.-L. Palmer, P.C. Sachs, R.D. Bruno, 3D bioprinted mammary organoids and tumoroids in human mammary derived ECM hydrogels, Acta Biomater. 95 (2019) 201–213, https://doi.org/10.1016/j.actbio.2019.06.017.
[42] G. Landberg, P. Fitzpatrick, P. Isakson, E. Jonasson, J. Karlsson, E. Larsson, A. Svanstro¨m, S. Rafnsdottir, E. Persson, A. Gustafsson, D. Andersson, J. Rosendahl, S. Petronis, P. Ranji, P. Gregersson, Y. Magnusson, J. Håkansson, A. Ståhlberg, Patient-derived scaffolds uncover breast cancer promoting properties of the microenvironment, Biomaterials 235 (2020), 119705, https://doi.org/10.1016/j.biomaterials.2019.119705.
[43] V.M. Gaspar, P. Lavrador, J. Borges, M.B. Oliveira, J.F. Mano, Advanced bottom-up engineering of living architectures, Adv. Mater. (2019), 1903975.
[44] F. Louis, S. Kitano, J.F. Mano, M. Matsusaki, 3D collagen microfibers stimulate the functionality of preadipocytes and maintain the phenotype of mature adipocytes for long term cultures, Acta Biomater. 84 (2019) 194–207, https://doi.org/10.1016/j.actbio.2018.11.048.
[45] A.A.N. Bruyneel, C.A. Carr, Ambiguity in the presentation of decellularized tissue composition: the need for standardized approaches, Artif. Organs 41 (2017) 778–784, https://doi.org/10.1111/aor.12838.
[46] L.P. Ferreira, V.M. Gaspar, J.F. Mano, Bioinstructive microparticles for self- assembly of mesenchymal stem Cell-3D tumor spheroids, Biomaterials 185 (2018) 155–173, https://doi.org/10.1016/j.biomaterials.2018.09.007.
[47] K. Froehlich, J.D. Haeger, J. Heger, J. Pastuschek, S.M. Photini, Y. Yan, A. Lupp, C. Pfarrer, R. Mrowka, E. Schleußner, U.R. Markert, A. Schmidt, Generation of multicellular breast cancer tumor spheroids: comparison of different protocols, J. Mammary Gland Biol. Neoplasia 21 (2016) 89–98, https://doi.org/10.1007/ s10911-016-9359-2.
[48] E.C. Costa, V.M. Gaspar, P. Coutinho, I.J. Correia, Optimization of liquid overlay technique to formulate heterogenic 3D co-cultures models, Biotechnol. Bioeng. 111 (2014) 1672–1685, https://doi.org/10.1002/bit.25210.
[49] M. Plaster, S. Singh, H. Tavana, Fibroblasts promote proliferation and matrix invasion of breast cancer cells in Co-culture models, Adv. Ther. 1900121 (2019), 1900121, https://doi.org/10.1002/adtp.201900121.

[50] D.P. Ivanov, T.L. Parker, D.A. Walker, C. Alexander, M.B. Ashford, P.R. Gellert, M. C. Garnett, Multiplexing spheroid volume, resazurin and acid phosphatase viability assays for high-throughput screening of tumour spheroids and stem cell neurospheres, PLoS One 9 (2014) 1–14, https://doi.org/10.1371/journal. pone.0103817.

[51] H. Hardelauf, J.-P. Frimat, J.D. Stewart, W. Schormann, Y.-Y. Chiang, P. Lampen, J. Franzke, J.G. Hengstler, C. Cadenas, L.A. Kunz-Schughart, J. West, Microarrays for the scalable production of metabolically relevant tumour spheroids: a tool for modulating chemosensitivity traits, Lab Chip 11 (2011) 419–428, https://doi. org/10.1039/C0LC00089B.

[52] S. Kostidis, R.D. Addie, H. Morreau, O.A. Mayboroda, M. Giera, Quantitative NMR analysis of intra-and extracellular metabolism of mammalian cells: a tutorial, Anal. Chim. Acta 980 (2017) 1–24.

[53] D.S. Wishart, D. Tzur, C. Knox, R. Eisner, A.C. Guo, N. Young, D. Cheng, K. Jewell, D. Arndt, S. Sawhney, HMDB: the human metabolome database, Nucleic Acids Res. 35 (2007) D521–D526.

[54] W.-H. Jung, N. Yam, C.-C. Chen, K. Elawad, B. Hu, Y. Chen, Force-dependent Extracellular Matrix Remodeling by Early-Stage Cancer Cells Alters Diffusion and Induces Carcinoma-Associated Fibroblasts, Biomaterials (2020), 119756..

[55] G. Rijal, J. Wang, I. Yu, D. Gang, R. Chen, W. Li, Porcine breast extracellular matrix hydrogel for spatial tissue culture, Int. J. Mol. Sci. 19 (2018) 2912, https://doi.org/10.3390/ijms19102912.

[56] S. Cebotari, I. Tudorache, T. Jaekel, A. Hilfiker, S. Dorfman, W. Ternes, A. Haverich, A. Lichtenberg, Detergent decellularization of heart valves for tissue engineering: toxicological effects of residual detergents on human endothelial cells, Artif. Organs 34 (2010) 206–210, https://doi.org/10.1111/j.1525- 1594.2009.00796.x.

[57] Y.C. Choi, J.S. Choi, B.S. Kim, J.D. Kim, H.I. Yoon, Y.W. Cho, Decellularized extracellular matrix derived from porcine adipose tissue as a xenogeneic biomaterial for tissue engineering, Tissue Eng. C Methods 18 (2012) 866–876, https://doi.org/10.1089/ten.tec.2012.0009.

[58] G. Rijal, W. Li, A versatile 3D tissue matrix scaffold system for tumor modeling and drug screening, Sci. Adv. 3 (2017) 1–17, https://doi.org/10.1126/ sciadv.1700764.

[59] L.B. Weiswald, D. Bellet, V. Dangles-Marie, Spherical cancer models in tumor biology, Neoplasia 17 (2015) 1–15, https://doi.org/10.1016/j.neo.2014.12.004.

[60] E.M. De Kruijf, J.G.H. Van Nes, C.J.H. Van De Velde, H. Putter, V.T.H.B.M. Smit, G.J. Liefers, P.J.K. Kuppen, R.A.E.M. Tollenaar, W.E. Mesker, Tumor-stroma ratio in the primary tumor is a prognostic factor in early breast cancer patients, especially in triple-negative carcinoma patients, Breast Canc. Res. Treat. 125 (2011) 687–696, https://doi.org/10.1007/s10549-010-0855-6.

[61] C.L. Downey, H.H. Thygesen, N. Sharma, A.M. Shaaban, Prognostic significance of tumour stroma ratio in inflammatory breast cancer, SpringerPlus 4 (2015) 3, https://doi.org/10.1186/s40064-015-0852-7.

[62] F. Montenegro, S. Indraccolo, Metabolism in the tumor microenvironment, Adv. Exp. Med. Biol. 1263 (2020) 1–11, https://doi.org/10.1007/978-3-030-44518-8_ 1.

[63] G. Peng, Y. Liu, Hypoxia-inducible factors in cancer stem cells and inflammation, Trends Pharmacol. Sci. 36 (2015) 374–383, https://doi.org/10.1016/j. tips.2015.03.003.

[64] D. Rodenhizer, T. Dean, B. Xu, D. Cojocari, A.P. McGuigan, A three-dimensional engineered heterogeneous tumor model for assessing cellular environment and response, Nat. Protoc. 13 (2018) 1917–1957, https://doi.org/10.1038/s41596- 018-0022-9.

[65] J.E. Reing, B.N. Brown, K.A. Daly, J.M. Freund, T.W. Gilbert, S.X. Hsiong, A. Huber, K.E. Kullas, S. Tottey, M.T. Wolf, S.F. Badylak, The effects of processing methods upon mechanical and biologic properties of porcine dermal extracellular matrix scaffolds, Biomaterials 31 (2010) 8626–8633, https://doi.org/10.1016/J. BIOMATERIALS.2010.07.083.

[66] K. Stock, M.F. Estrada, S. Vidic, K. Gjerde, A. Rudisch, V.E. Santo, M. Barbier, S. Blom, S.C. Arundkar, I. Selvam, A. Osswald, Y. Stein, S. Gruenewald, C. Brito, W. van Weerden, V. Rotter, E. Boghaert, M. Oren, W. Sommergruber, Y. Chong, R. de Hoogt, R. Graeser, Capturing tumor complexity in vitro: comparative analysis of 2D and 3D tumor models for drug discovery, Sci. Rep. 6 (2016) 28951, https://doi.org/10.1038/srep28951.

[67] M.F. Gencoglu, L.E. Barney, C.L. Hall, E.A. Brooks, A.D. Schwartz, D.C. Corbett, K. R. Stevens, S.R. Peyton, Comparative study of multicellular tumor spheroid formation methods and implications for drug screening, ACS Biomater. Sci. Eng. (2017), 7b00069, https://doi.org/10.1021/acsbiomaterials.7b00069 acsbiomaterials.

[68] D.L. Holliday, V. Speirs, Choosing the right cell line for breast cancer research, Breast Canc. Res. 13 (2011) 1–7, https://doi.org/10.1186/bcr2889.

[69] X. Dai, H. Cheng, Z. Bai, J. Li, Breast cancer cell line classification and its relevance with breast tumor subtyping, J. Canc. 8 (2017) 3131–3141, https://doi. org/10.7150/jca.18457.

[70] H.R. Ali, H.W. Jackson, V.R.T. Zanotelli, E. Danenberg, J.R. Fischer, H. Bardwell, E. Provenzano, O.M. Rueda, S.-F. Chin, S. Aparicio, C. Caldas, B. Bodenmiller, Imaging mass cytometry and multiplatform genomics define the phenogenomic landscape of breast cancer, Nat. Canc. 1 (2020) 163–175, https://doi.org/ 10.1038/s43018-020-0026-6.

[71] S. Qiu, R. Hong, Z. Zhuang, Y. Li, L. Zhu, X. Lin, Q. Zheng, S. Liu, K. Zhang, M. Huang, K. Lee, Q. Lu, W. Xia, F. Xu, X. Wang, J. Tang, X. Xiao, W. Wei, Z. Yuan, Y. Shi, Y. Hou, X. Zhang, J. Wang, H. Yang, Q. Zhan, B. Li, S. Wang, A single-cell immune atlas of triple negative breast cancer reveals novel immune cell subsets, BioRxiv (2019) 566968, https://doi.org/10.1101/566968.

[72] H.W. Jackson, J.R. Fischer, V.R.T. Zanotelli, H.R. Ali, R. Mechera, S.D. Soysal, H. Moch, S. Muenst, Z. Varga, W.P. Weber, B. Bodenmiller, The single-cell pathology landscape of breast cancer, Nature (2020), https://doi.org/10.1038/ s41586-019-1876-x.

[73] M.E. Fiori, S. Di Franco, L. Villanova, P. Bianca, G. Stassi, R. De Maria, Cancer- associated fibroblasts as abettors of tumor progression at the crossroads of EMT and therapy resistance, Mol. Canc. 18 (2019) 1–16, https://doi.org/10.1186/ s12943-019-0994-2.

[74] T. Ahmad, J. Lee, Y.M. Shin, H.J. Shin, S.K.M. Perikamana, S.H. Park, S.W. Kim, H. Shin, Hybrid-spheroids incorporating ECM like engineered fragmented fibers potentiate stem cell function by improved cell/cell and cell/ECM interactions, Acta Biomater. 64 (2017) 161–175, https://doi.org/10.1016/j. actbio.2017.10.022.

[75] M. Grossman, N. Ben-Chetrit, A. Zhuravlev, R. Afik, E. Bassat, I. Solomonov, Y. Yarden, I. Sagi, Tumor cell invasion can be blocked by modulators of collagen fibril alignment that control assembly of the extracellular matrix, Cancer Res. 76 (2016) 4249–4258.

[76] J. Insua-Rodríguez, T. Oskarsson, The extracellular matrix in breast cancer, Adv. Drug Deliv. Rev. 97 (2016) 41–55, https://doi.org/10.1016/j.addr.2015.12.017.

[77] M. Cavo, M. Caria, I. Pulsoni, F. Beltrame, M. Fato, S. Scaglione, A new cell-laden 3D Alginate-Matrigel hydrogel resembles human breast cancer cell malignant morphology, spread and invasion capability observed “in vivo, Sci. Rep. 8 (2018) 1–12.

[78] I. Acerbi, L. Cassereau, I. Dean, Q. Shi, A. Au, C. Park, Y.Y. Chen, J. Liphardt, E. S. Hwang, V.M. Weaver, Human breast cancer invasion and aggression correlates with ECM stiffening and immune cell infiltration, Integr. Biol. (United Kingdom). 7 (2015) 1120–1134, https://doi.org/10.1039/c5ib00040h.

[79] M. Giussani, G. Merlino, V. Cappelletti, E. Tagliabue, M.G. Daidone, Tumor- extracellular matrix interactions: identification of tools associated with breast cancer progression, Semin. Canc. Biol. 35 (2015) 3–10, https://doi.org/10.1016/ j.semcancer.2015.09.012.

[80] H. Li, Z. Qiu, F. Li, C. Wang, The relationship between MMP-2 and MMP-9 expression levels with breast cancer incidence and prognosis, Oncol. Lett. 14 (2017) 5865–5870, https://doi.org/10.3892/ol.2017.6924.

[81] R.L. Furler, D.F. Nixon, C.A. Brantner, A. Popratiloff, C.H. Uittenbogaart, TGF-β sustains tumor progression through biochemical and mechanical signal transduction, Cancers 10 (2018) 1–18, https://doi.org/10.3390/ cancers10060199.

[82] G. Xiao, X. Wang, J. Wang, L. Zu, G. Cheng, M. Hao, X. Sun, Y. Xue, J. Lu, J. Wang, CXCL16/CXCR6 chemokine signaling mediates breast cancer progression by pERK1/2-dependent mechanisms, Oncotarget 6 (2015) 14165–14178, https://doi.org/10.18632/oncotarget.3690.

[83] L.M. Martins, C.S. de Melo Escorcio Dourado, L.M. Campos-Verdes, F.A. Sampaio,

C.M.S. Revoredo, D.R. Costa-Silva, M. da Conceiça˜o Barros-Oliveira, E. de Jesus Nery Junior, L.M. do Rego-Medeiros, L.H. Gebrim, F.A. Alves-Ribeiro, G.
P. Rodrigues, D.C. Chagas, D. do Nascimento Marreiro, B.B. Da Silva, Expression of matrix metalloproteinase 2 and 9 in breast cancer and breast fibroadenoma: a randomized, double-blind study, Oncotarget 10 (2019) 6879–6884, https://doi. org/10.18632/oncotarget.27347.

[84] P. Kunz, H. S¨ahr, B. Lehner, C. Fischer, E. Seebach, J. Fellenberg, Elevated ratio of MMP2/MMP9 activity is associated with poor response to chemotherapy in osteosarcoma, BMC Canc. 16 (2016) 1–10, https://doi.org/10.1186/s12885-016- 2266-5.

[85] S. Ławicki, M. Zajkowska, E.K. Głażewska, G.E. Będkowska, M. Szmitkowski, Plasma levels and diagnostic utility of VEGF, MMP-2 and TIMP-2 in the diagnostics of breast cancer patients, Biomarkers 22 (2017) 157–164, https://doi. org/10.1080/1354750X.2016.1252955.

[86] X. Lei, A. Bandyopadhyay, T. Le, L.Z. Sun, Autocrine TGFβ supports growth and survival of human breast cancer MDA-MB-231 cells, Oncogene 21 (2002) 7514–7523, https://doi.org/10.1038/sj.onc.1205966.

[87] M.H. Barcellos-Hoff, R.J. Akhurst, Transforming growth factor-β in breast cancer: too much, too late, Breast Canc. Res. 11 (2009), https://doi.org/10.1186/ bcr2224.

[88] D. Bourboulia, W.G. Stetler-Stevenson, Matrix metalloproteinases (MMPs) and tissue inhibitors of metalloproteinases (TIMPs): positive and negative regulators in tumor cell adhesion, Semin. Canc. Biol. 20 (2010) 161–168, https://doi.org/ 10.1016/j.semcancer.2010.05.002.

[89] S. Busch, A. Acar, Y. Magnusson, P. Gregersson, L. Ryd´en, G. Landberg, TGF-beta receptor type-2 expression in cancer-associated fibroblasts regulates breast cancer cell growth and survival and is a prognostic marker in pre-menopausal breast cancer, Oncogene 34 (2015) 27–38, https://doi.org/10.1038/onc.2013.527.

[90] G.J. Yoshida, Regulation of heterogeneous cancer-associated fibroblasts: the molecular pathology of activated signaling pathways, J. Exp. Clin. Canc. Res. 39 (2020) 112, https://doi.org/10.1186/s13046-020-01611-0.

[91] B. Hinz, The extracellular matrix and transforming growth factor-β1: tale of a strained relationship, Matrix Biol. 47 (2015) 54–65, https://doi.org/10.1016/j. matbio.2015.05.006.

[92] K. Liang, Y. Liu, D. Eer, J. Liu, F. Yang, K. Hu, High CXC chemokine ligand 16 (CXCL16) expression promotes proliferation and metastasis of lung cancer via regulating the NF-κb pathway, Med. Sci. Mon. Int. Med. J. Exp. Clin. Res. 24 (2018) 405–411, https://doi.org/10.12659/MSM.906230.

[93] T. Ukaji, Y. Lin, S. Okada, K. Umezawa, Inhibition of MMP-2-mediated cellular invasion by NF-κB inhibitor DHMEQ in 3D culture of breast carcinoma MDA-MB- 231 cells: a model for early phase of metastasis, Biochem. Biophys. Res. Commun. 485 (2017) 76–81, https://doi.org/10.1016/j.bbrc.2017.02.022.

[94] A.G. Waks, E.P. Winer, Breast cancer treatment: a review, JAMA - J. Am. Med. Assoc. 321 (2019) 288–300, https://doi.org/10.1001/jama.2018.19323.

[95] Z.I. Khamis, Z.J. Sahab, Q.-X.A. Sang, Active roles of tumor stroma in breast cancer metastasis, Int. J. Breast Canc. 2012 (2012).

[96] G. Finak, N. Bertos, F. Pepin, S. Sadekova, M. Souleimanova, H. Zhao, H. Chen, G. Omeroglu, S. Meterissian, A. Omeroglu, Stromal gene expression predicts clinical outcome in breast cancer, Nat. Med. 14 (2008) 518–527.

[97] S. Skolekova, M. Matuskova, M. Bohac, L. Toro, L. Demkova, J. Gursky, L. Kucerova, Cisplatin-induced mesenchymal stromal cells-mediated mechanism contributing to decreased antitumor effect in breast cancer cells, Cell Commun. Signal. 14 (2016) 1–13, https://doi.org/10.1186/s12964-016-0127-0.

[98] M. Majidinia, B. Yousefi, Breast tumor stroma: a driving force in the development of resistance to therapies, Chem. Biol. Drug Des. 89 (2017) 309–318, https://doi. org/10.1111/cbdd.12893.

[99] M. Wang, Z.M. Liu, X.C. Li, Y.T. Yao, Z.X. Yin, Activation of ERK1/2 and Akt is associated with cisplatin resistance in human lung cancer cells, J. Chemother. 25 (2013) 162–169, https://doi.org/10.1179/1973947812Y.0000000056.

[100] K. Gohr, A. Hamacher, L.H. Engelke, M.U. Kassack, Inhibition of PI3K/Akt/mTOR overcomes cisplatin resistance in the triple negative breast cancer cell line HCC38, BMC Canc. 17 (2017) 1–13, https://doi.org/10.1186/s12885-017-3695- 5.

[101] C.M. Rocha, A.S. Barros, B.J. Goodfellow, I.M. Carreira, A. Gomes, V. Sousa, J. Bernardo, L. Carvalho, A.M. Gil, I.F. Duarte, NMR metabolomics of human lung tumours reveals distinct metabolic signatures for adenocarcinoma and squamous cell carcinoma, Carcinogenesis 36 (2015) 68–75.

[102] C. Denkert, E. Bucher, M. Hilvo, R. Salek, M. Oreˇsiˇc, J. Griffin, S. Brockmo¨ller, F. Klauschen, S. Loibl, D.K. Barupal, Metabolomics of human breast cancer: new approaches for tumor typing and biomarker discovery, Genome Med. 4 (2012) 37.

[103] A.E. Place, S.J. Huh, K. Polyak, The microenvironment in breast cancer progression: biology and implications for treatment, Breast Cancer Res. 13 (2011) 227.

[104] M.R. Cardoso, J.C. Santos, M.L. Ribeiro, M.C.R. Talarico, L.R. Viana, S.F. M. Derchain, A metabolomic approach to predict breast cancer behavior and chemotherapy response, Int. J. Mol. Sci. 19 (2018) 617.

[105] A.K. Witkiewicz, D. Whitaker-Menezes, A. Dasgupta, N.J. Philp, Z. Lin, R. Gandara, S. Sneddon, U.E. Martinez-Outschoorn, F. Sotgia, M.P. Lisanti, Using the "reverse Warburg effect" to identify high-risk breast cancer patients: stromal MCT4 predicts poor clinical outcome in triple-negative breast cancers, Cell Cycle 11 (2012) 1108–1117.

[106] F. Tayyari, G.A.N. Gowda, O.F. Olopade, R. Berg, H.H. Yang, M.P. Lee, W. F. Ngwa, S.K. Mittal, D. Raftery, S.I. Mohammed, Metabolic profiles of triple-negative and luminal A breast cancer subtypes in African-American identify key metabolic differences, Oncotarget 9 (2018) 11677–11690, https://doi.org/ 10.18632/oncotarget.24433.

[107] E. Borgan, B. Sitter, O.C. Lingjærde, H. Johnsen, S. Lundgren, T.F. Bathen, T. Sørlie, A.-L. Børresen-Dale, I.S. Gribbestad, Merging transcriptomics and metabolomics-advances in breast cancer profiling, BMC Canc. 10 (2010) 628.

[108] J.E. Bader, K. Voss, J.C. Rathmell, Targeting metabolism to improve the tumor microenvironment for Cancer immunotherapy, Mol. Cell. 78 (2020) 1019–1033.

[109] N. Sugandha, L. Mittal, A. Awasthi, S. Asthana, Recent advances in drug development targeting cancer metabolism. Cancer Cell Metab. A Potential Target Cancer Ther., Springer, 2020, pp. 103–126.

[110] G. Hoxhaj, B.D. Manning, The PI3K–AKT network at the interface of oncogenic signalling and cancer metabolism, Nat. Rev. Canc. 20 (2020) 74–88.